

An Analysis of Using a Subcritical Reactor Design to Produce Molybdenum-99 using Uranium Targets

Peter Hotvedt, Tomas Montenegro, Noah Schweitzer

University of Wisconsin-Madison

Department of Engineering Physics

Instructors: John Murphy, Tim Bohm

July 31, 2020



**Department of
Engineering Physics**
UNIVERSITY OF WISCONSIN-MADISON

Executive Summary

Metastable Technetium-99, or ^{99m}Tc , is used in approximately 40 million diagnostic procedures annually in the United States making it a healthcare necessity. Utilization of ^{99m}Tc in diagnostic procedures include SPECT scans, PET scans, Myocardial Perfusion Imaging (MPI), and other imaging processes. Although the demand for the radioisotope is large, the supply is insufficient and unreliable for future demands. In order to obtain ^{99m}Tc , the parent isotope, ^{99}Mo , is produced in a reactor setting. As of July 2017, there are only six research reactors across six different countries, none of which being the United States, that produce ^{99}Mo on a large scale. Several of these reactors are scheduled to be decommissioned in the near future, leading to a lack of certainty in the accessible supply of ^{99}Mo . Additionally, the majority of the reactors producing ^{99}Mo use High Enriched Uranium (HEU) fuel which poses a proliferation concern. Therefore, new ^{99}Mo production techniques must be developed to fill the supply and demand gap in the United States. This project aims to fill this void by developing a sub-critical reactor which has the means to supply a local hospital setting, in this case, the University of Wisconsin's UW Health Clinic System.

The design seeks to fill the main flaws of the existing techniques for producing ^{99}Mo . The developed system seeks to utilize Low Enriched Uranium (LEU) targets, maintain a k_{eff} below 0.99 to keep the reactor safely sub-critical, and optimize the production of ^{99}Mo with a minimum activity of 450 6-day curies, at least 1/10th of the total United States' present demand. With a sub-critical design, the system is designed to be driven by a Deuterium-Tritium (DT) neutron accelerator source which produces 1×10^{13} neutrons per second. The targets are then designed to be irradiated for a week, stored in cooling pits, and then sent to hot cells for a standard ^{99}Mo chemical extraction procedure.

With the initial design parameters in place, technical decisions had to be made on how to assemble the final product with regards to fuel type, and reactor geometry, among other quantities. First, the type LEU target with respect to chemical compound had to be selected. Uranium was chosen due to its high specific activity yield for ^{99}Mo that would make the design criteria of a subcritical reactor and the demand needed feasible, but it was critical to pick the proper Uranium compound that would work for our targeting system. Of the Uranium targets available, solid Uranium Dioxide (UO_2) was selected due to its high density, 9.7 g/cm^3 and proven extraction methods compared to the other Uranium targets. The targets were then designed through an iterative approach to achieve a 0.9867 multiplication constant. From this approach, the targets were designed to have a fuel region length of 49 cm and a radius of 1.5 cm, and then organized in a tight square lattice around the accelerator. To preserve the neutron economy in the target region, graphite reflectors were added to either side of the targets and along the outside perimeter of the assembly.

After the designs were finalized based on the criticality achieved, the outputs of the reactor were determined. It was found that the reactor achieves an operating power of 4.4 kW and a peak fuel temperature of 28°C , leading to a simplified cooling design

and a low risk of accidents. The average fission rate was determined to be 1.206×10^{12} fissions per second, a relatively low fission rate, leading to a low ^{99}Mo production of approximately 37 6-day curies per duty cycle (duty cycle is one week) which did not meet the design criteria.

While the end production goal was not met, the reactor itself had several strong safety features. One issue with switching to an LEU target is the high production of ^{239}Pu which in turn is a proliferation concern. This design produces a relatively low amount of ^{239}Pu at 4.53 mg per duty cycle. Additionally, the DPA rate does not reach 0.1 until 300 years, allowing the reactor to have a lifetime for at least this length. Furthermore, the maximum dose rates during operation were well below that of safety concerns, as the top and side of the pool were 0.618 and 0.062 mrem/hour, respectively. Overall, the design had a robust system capable of handling and reducing potential accidents needed for an in-house reactor.

Although the safety aspects were a success, producing only 37 6-day curies per week of ^{99}Mo was well below the design criteria of 450 6-day curies per week. The main issue with the system is that only 18% of the source neutrons induce fission. Meanwhile, SHINE Medical Technologies, another US company vying to compete for ^{99}Mo production, developed an aqueous solution of uranyl nitrate that utilizes 50% of the source neutrons to induce fission. The drastic difference in the percentage of source neutrons inducing fissions display that while the production of ^{99}Mo could most likely be improved in the design, it would still not reach the same production levels as that of SHINE. Additionally, the system designed would have trouble dealing with a scenario where there is significant fission product build up as there are no known means of removing poisons during operation. In conclusion, this work displays how a solid target, sub-critical reactor system is stable and has strong safety feature, but it is not feasible to produce enough ^{99}Mo needed for the UW Hospital System, let alone United States' demand.

Contents

Executive Summary	i
List of Figures	vii
List of Tables	viii
1 Introduction	1
1.1 Background	1
1.2 Problem Statement	4
1.3 Design Objectives and Specifications	5
1.4 Context and Significance of Design	6
1.5 Report Layout	7
2 Design Summary: Process and Methods	9
2.1 Initial Technical Specifications	9
2.2 Molybdenum-99 Production via Reactions	12
2.3 Material Decisions	13
2.4 Accelerator Information	14
2.5 Design Refinements	14
2.6 Design and Project Limitations	16
2.7 Design Parameters	18
3 Molybdenum-99 Production Process	19

3.1	Duty Cycle	19
3.2	Target Production and Irradiation Process	20
3.3	Cooling Stage	20
3.4	Chemical Treatment	21
3.5	Transportation Methods	23
3.6	Summary and Rate Equation	23
4	Neutronic Analysis	25
4.1	Hand Calculations	25
4.2	Initial Homogeneous Reactors	29
4.3	Accelerator Source Modelling	30
4.4	Detail and Sizing Progression	31
4.4.1	Finalized Assembly Geometry	34
4.5	Flux Profile	37
4.6	Final ^{99}Mo Production	41
4.7	Reasons for Failure	44
5	Shielding Analysis	47
5.1	Choice of Material	48
5.2	Dose Calculations and Pool Sizing	49
5.3	Extraction and Transportation Shielding	51
5.4	Storage and Transportation of Radioisotopes	54
6	Thermal Considerations	55
6.1	Thermal Analysis of the Core	55
7	Safety Considerations	63
7.1	Potential Safety and Accident Scenarios	64
7.1.1	Accidental Loading of Extra Targets	64

7.1.2	Change in Moderator Density	67
7.1.3	Loss of Coolant / Moderator	67
7.1.4	Loss of Heat Sink	68
7.2	Safety Poison Injection and Reactor Shutdown Conditions	69
7.3	DPA Analysis	72
7.4	Cooling and Storage Pit	73
7.5	Plutonium Production	76
8	Economic Considerations	77
8.1	Economic Considerations	77
9	Conclusion	79
9.1	Key Design Features	80
9.1.1	Target Material Choices	80
9.1.2	Assembly Geometry	80
9.1.3	Shielding	81
9.1.4	Thermal Analysis	82
9.1.5	Safety Analysis	82
9.1.6	Cost	83
9.2	Future Work and Improvements	83
10	Acknowledgements	86
	References	87
A	MATLAB Code	90
A.1	Plotting Thermal Tallies	90
B	MCNP6 Script	95

List of Figures

2.1	Top-down view of the hexagonal lattice scheme	15
2.2	Top-down view of an initial target distribution in a square scheme	16
3.1	Hot Cells in use for processing Mo-99 from an LEU source. [9]	21
3.2	(a) a view into the Hot Cell and (b) a view of the dissolving agents used in the chemical treatment process [9]	22
4.1	Table presenting activation risks of different elements	34
4.2	Top down view of the assembly	35
4.3	Side view of the assembly	36
4.4	Side view of individual targets	37
4.5	Neutron flux as function of radial position plotted over assembly geometry	38
4.6	Flux profile plotted over side view of assembly to show axial dependence of neutron flux	38
4.7	Neutron flux as a function of radial position in assembly	39
4.8	Neutron flux as a function of radial position in the assembly divided into three energy groups	40
4.9	Fission product yields for different fission reactions. The red dot marks the ⁹⁹ Mo yield.	42
4.10	Color bar plot of fissions per second in each target pin	43
5.1	Radiation zoning used to limit time spent in radiation areas [14]	47
5.2	Pool top photon dose rates as a function of pool depth	51

5.3	Linear attenuation coefficients for shielding materials as a function of energy [18]	53
6.1	Original heat density tallies recorded in MCNP	56
6.2	A vertical cross-section of the heat density tally	57
6.3	The vertical slice of the heat density in Figure (6.2) revolved about the vertical axis	57
6.4	The horizontal heat density cross-section at 28.5 cm	58
6.5	The horizontal heat density cross-section at 31.5 cm	59
6.6	The horizontal heat density cross-section at 58.5 cm	59
6.7	Grainger's Heat Exchanger that will be utilized is displayed [19]	61
6.8	The Fuel Pins' in-core heating	62
7.1	The locations of accident scenarios analyzed. Green elements show accidentally inserted targets and the numbers show the corresponding grid location	65
7.2	Gadolinium neutron cross-section as a function of incident neutron energy	71
7.3	The results of the DPA Tally on the Gridbox mesh	73
7.4	Close up of storage pit showing concrete and boron carbide dividers	74
7.5	Top down view of cooling pit. The pit is 120 cm × 30 cm	74
7.6	Side view of storage pit	75

List of Tables

2.1	The relative ^{99}Mo yield from varying nuclear reactions	12
2.2	Design Summary Table	18
4.1	Homogeneous UO_2 and H_2O reactor characteristics	29
4.2	Simple Tube reactor characteristics	30
4.3	Homogeneous UO_2 and H_2O reactor characteristics	33
4.4	Homogeneous UO_2 and H_2O reactor characteristics	35
4.5	Homogeneous UO_2 and H_2O reactor characteristics	36
4.6	Key dimensions of target	37
4.7	Key dimensions of target	41
4.8	Homogeneous UO_2 and H_2O reactor characteristics	44
7.1	Criticality Calculations for accident scenarios described in Figure 7.1	65
7.2	Reactivity effects of changes to water temperature and density	67
7.3	Dose rates with assembly uncovered	68
7.4	Conditions initiating either automatic accelerator shutoff of neutron poison injection	70

Chapter 1

Introduction

1.1 Background

Metastable Technetium-99, or ^{99m}Tc is a very important isotope in the field of medicine. Unlike other isotopes of Technetium, ^{99m}Tc has the unique trait of having its nucleus remain in an excited state far longer than other isotopes of Tc (hence the term “metastable”). Though, like all other isotopes, ^{99m}Tc eventually returns to a ground state, though in doing so it either emits a gamma ray (approximately 88% of the time) or undergoes internal conversion (approximately 12% of the time). Through the more common means of decay, ^{99m}Tc emits a gamma with an energy of approximately 140.5 keV approximately 98% of the time. During this roughly six hour period before a decay to ground state, the emitted gammas can be picked up using devices known as Gamma Cameras and be converted to images for diagnostic procedures. Given that most of the dose to the patient comes from the internal conversion process, which is a far less common process than gamma emission, as well as the previously alluded to fact that ^{99m}Tc has a

half life of approximately 6 hours, ^{99m}Tc happens to be one of the useful radioisotopes for diagnostic procedures. It should be noted as well that after decaying into ^{99}Tc , the new radioisotope is very stable and very safe as it emits low energy beta particles which makes it considerable useful for pharmaceuticals. ^{99m}Tc is used in a wide variety of diagnostic procedures, such as SPECT scans, PET scans, Myocardial Perfusion Imaging (MPI), and other imaging processes, and as such there is a significant demand for the isotope. Given that approximately 40 million diagnostic procedures annually use ^{99m}Tc , (about 80% of all diagnostic processes in the United States) [1], the high demand has lead to an inevitable shortage of the radioisotope. This depletion of materials begs the question: “How can hospitals get more ^{99m}Tc ?”.

The process of producing more ^{99m}Tc is notably straightforward as ^{99m}Tc itself is the daughter isotope of another radioisotope, Molybdenum-99 (or ^{99}Mo). ^{99}Mo is gathered from its parent isotope and manufactured such that it can be shipped to hospitals that are in need. The transportation process is done as ^{99}Mo instead of ^{99m}Tc as ^{99}Mo has a noticeably longer half-life, approximately 66 hours or 2 days, compared to its daughter isotope. However, a 2 day period is still a small window for shipping a large quantity of ^{99}Mo , so the isotope must be manufactured and transported efficiently. What separates ^{99}Mo from other radioisotopes that might have appropriate daughter particles for nuclear imaging, or longer half lives making for easier manufacture and transport, is the fact that ^{99}Mo is also a common fission product of Uranium-235 (^{235}U), which is an extremely common fuel used in reactors. In particular, when ^{235}U is bombarded by thermal neutrons or 14.1 MeV neutrons, there is a 6% and 5% fission yield percentage respectively. Therefore, in order to maximize the amount of ^{99}Mo being manufactured and shipped, those producing the radioisotope must optimize the reactors they use in

order to verify that the neutrons bombarding the source are at the proper energies.

However, the process of gathering ^{99}Mo as a fission product from various reactors presents a problem. Of the many currently operating reactors, very few are currently equipped with the means of gathering ^{99}Mo in the way that a specialized reactor for this process might. While there are new startup companies like SHINE and Northstar constructing facilities to produce ^{99}Mo , as well as pharmaceutical companies such as Coquí RadioPharmaceuticals working with National Labs like Oak Ridge to construct their own production facilities, as of July 2017 there are only six research reactors across six different countries, none of which being the United States, that produce ^{99}Mo on a large scale. Furthermore, a majority of the aforementioned reactors use High Enriched Uranium (HEU) fuel as opposed to Low Enriched Uranium (LEU) fuel [2], and are very old and are on their way towards being decommissioned. With regards to the United States and ^{99}Mo production, licensed HEU exports for the medical use of ^{99}Mo presently are allowed, however this prospect is unlikely to last. While as of January 21, 2020, the National Nuclear Security Administration (NNSA), a branch of the U.S. Department of Energy (DoE), certified that

“there is an insufficient global supply of molybdenum-99 produced without the use of highly enriched uranium available to satisfy the domestic U.S. market and that the export of U.S.-origin highly enriched uranium for the purposes of medical isotope production is the most effective temporary means to increase the supply of molybdenum-99 to the domestic U.S. market.” [3]

This fix, however, is a temporary patch however as the certification only lasts for two years until 2022. therefore a long-term domestic solution involving LEU is necessary.

1.2 Problem Statement

This project focuses on the creation of a sub-critical nuclear reactor designed to produce enough ^{99}Mo to supply to a local hospital setting, in this case the University of Wisconsin's UW Health clinic. The subcritical reactor must be able to produce at least 450 6-day curies per week, approximately 1/10 of the total United States' present demand, using LEU targets as fuel. A 6-day curie is defined as the measurement of remaining activity of ^{99}Mo exactly six days after it is removed from the processing facility at the end of the creation duty cycle. While this value is a guideline, the overall goal is to effectively optimize the system to produce as much ^{99}Mo as possible, while still meeting the prescribe 450 6-day curie per week minimum. The product from the reactor also needs to be in a form that can be used with Technetium Generators commonly used in hospital settings.

While there are no general locations on campus upon which this reactor would be built, this project acts more as a hypothetical situation at a local location. The distance however, would be considered near negligible for the sake of simplicity in calculations, especially when compared to the scale in distance to companies like SHINE and NorthStar that ship their products across the United States. There is also the case of the chemical treatment facility that would need to be constructed in a similar location. However, like the issue with the location of the reactor, the planning of a location for the UW-Health system is beyond the scope of this project. Additionally, like with the reactor component, the assumed travel time between the two locations is to be near negligible (an hour at most) compared to other ^{99}Mo production facilities and consumption locations.

1.3 Design Objectives and Specifications

As previously noted, the ^{99}Mo that is being produced needs to adhere to a certain specific design requirements. First, and foremost, the reactor must remain sub-critical during all period of operation. The choice to maintain a $k_{eff} < 1$ is done primarily to ensure the safe of nearby locations such as the hospital will be moving its product to, as well as to quell any public concerns of having a reactor close to a medical facility. While the project itself does not go into the efforts of a persuading the public to be alright with the construction of a subcritical nuclear reactor seemingly right in the middle of a suburban area, safety considerations need to consistently be a top priority. Operating at a low power, subcritical state is a notably safer state and operating close to or at a critical state, which can therefore prioritize safety in the event of an accident. Therefore, the reactor also can also operate at a notably lower power level compared to a reactor designed to provide power to a specific energy market.

One of the primary design focuses is that the fuel must be LEU targets. This is chosen as opposed to a homogeneous solution for fuel for a number of reasons, though most have to do with the safety of operation and maintaining the reactor in a subcritical state. There are many benefits of using targets as opposed to a solution, which include, but are not limited to: the fact that LEU targets will not produce radioactive uranium salts in the bottom of the reactor's core caused by oxidation with water, the targets themselves are often quite easy to replace and maintain, and that it is far easier to transport targets to and from locations safely. The choice of having a low-enriched material is also a conscious one, mainly due to the specific control on high-enriched uranium fuels. Per NRC Regulation §50.64, for domestic non-power reactors, the NRC will

not issue a construction permit for reactors that use HEU, unless “unless the applicant demonstrates that the proposed reactor will have a unique purpose as defined in §50.2” [4]. The definition as outlined in §50.2 defines a unique purpose as “a project, program, or commercial activity which cannot reasonably be accomplished without the use of HEU fuel” [5]. While this process could theoretically be done with HEU, HEU is not absolutely required for the production process of ^{99}Mo . Therefore, the reactor is required to use LEU, though the enrichment for the targets can be chosen to be as high or low as necessary so long as it remains below the given boundary (Target Enrichment $< 20\%$). Furthermore, the targets used in this design must be fabricated in a specific way such that they fit inside of the irradiation position of reactor, and must be able to have some sort of barrier to prevent the release of fission gasses or any other radioactive products that may present themselves after irradiation. Therefore it stands that the targets must have some kind of cladding applied during the target manufacture process. The material choices for the cladding will be investigated in greater detail later in the report, with a focus on making sure that the dimensions of the targets are appropriate for irradiation.

1.4 Context and Significance of Design

While there are existing companies and research reactors that produce ^{99}Mo , presently there are no ^{99}Mo -specific reactors that only produce on an in-house level. Given the shortage of ^{99m}Tc and the need for the imaging agent in all hospitals, the question of whether or not it would be economically viable, let alone feasible, to have a subcritical reactor on hand to produce ^{99}Mo . While there are developing projects that

focus on this type of target-based project, such as the previously mentioned Coquí RadioPharmaceuticals project, this type of project and potential solution is still a relatively new one. As it stands, while there are similar existing results, much of the processes and existing data are proprietary so the verification of our results may be somewhat difficult. One of the other challenges facing the radiopharmaceutical industry was the previously alluded to fact that there are minimal reactors producing ^{99}Mo , and those that are producing the radioisotope are aging reactors. The closure of many of these reactors poses an immediate problem that needs to be solved within the next 10-20 years, as many of the current ^{99}Mo producing reactors are likely to be decommissioned in that time frame. And while more and more pharmaceutical companies and startups are beginning to develop technologies to produce ^{99}Mo , it is worth investigating whether or not an in-house ^{99}Mo producing reactor would be economically viable against the new sources.

1.5 Report Layout

This report will first cover the background details about the project as a whole, including design justifications supplemented and supported by nuclear physics. Equations such as the six-factor formula, material buckling and other, otherwise commonplace, equations will be presented in order to establish a foundation for decision making processes for the reader's convenience. This section also will lay out a variety of different design choice explanations as well as some limitations in the overall design. The report will then go through the designed production process. A duty cycle will be presented and then observed in more depth in order to understand the full production process of ^{99}Mo . Some of these steps presented include the irradiation process of the targets, the

cooling of the targets after irradiation, and the chemical extraction process. The report will then cover technical investigations into the neutronics, shielding, thermal, safety and economic analyses of the project. The report will then conclude with a recapitulation of the technical aspects of the design and a discussion of the feasibility of the design as a whole.

Chapter 2

Design Summary: Process and Methods

2.1 Initial Technical Specifications

This design was inspired by the nearby presences of both Northstar and SHINE to campus. Given that two of the members of our group are majoring in the Radiation Sciences track of the Nuclear Engineering major, there was an attempt to find a project that had ties to the medical industry with respect to radioisotope usage. SHINE and Northstar's proximity to campus prompted the question of whether or not it would be feasible, or even possible, to create a reactor suitable for in-house production of Molybdenum-99 for eventual use as ^{99m}Tc in the nearby UW Hospital System, including hospitals like the University Hospital, the 1 South Park site and the Johnson Creek site.

From the problem statement, NRC specifications and safety factors, the fuel and

core materials had to be chosen very carefully. From the beginning, our design process always intended to yield a product that was very similar to existing cores such as those at SHINE and Northstar Medical Isotopes. There were, however, significant decisions and limitations that we had had to develop early on in order to avoid the scope of the project going to the furthest extreme. These decisions were essential guidelines that allowed us to formally develop an end goal and then explicitly work backwards to come to a full design process.

The first, and arguably most important design choice was determining the total amount of ^{99}Mo that we wanted to produce. From some of our research, the total amount of ^{99}Mo required for diagnostic procedures across the United States is approximately 5,000 6-day curies, and globally approximately 9,000 6-day curies [6]. This value is obviously an upper bound to the amount of ^{99}Mo required for the state of Wisconsin, let alone for the Dane County area, so we needed to determine a lower, more realistic quantity to produce. We opted to have our design create a fraction of the value for the entire U.S., that was initially 1/20th. This fraction was intended to cover the total possible amount of ^{99m}Tc needed at the UW Health System, which includes the main facility UW Health University, the 1 South Park site and the Johnson Creek site. After some early deliberation however, the fractional amount was eventually raised to 1/10th of the total requirement after considering that it would be better to optimize our system. Therefore, the design specification focused more on designing an optimal system to produce as much ^{99}Mo as possible, with a minimum guideline of 450 6-day curies per week.

The criticality of our system and means of keeping it at a certain effective multiplication factor (k_{eff}) were some of the most important design choices of the whole

project as well. For the reader's reference, the quantity k_{eff} is defined as:

$$k_{eff} = k_{\infty} P_{TNL} P_{FNL} \quad (2.1)$$

where P_{TNL} and P_{FNL} are the thermal and fast nonleakage probabilities (i.e. probabilities in which a thermal and fast neutron will not leak out of the system) respectively, and k_{∞} is defined in equation (2.2) as

$$k_{\infty} = \eta f p \epsilon \quad (2.2)$$

where

$$\eta = \nu \frac{\Sigma_{fuel}}{\Sigma_{fuel,abs}} \quad \equiv \text{The number of neutrons produced per neutrons absorbed by the fuel}$$

$$f = \frac{\Sigma_{fuel,abs}}{\Sigma_{abs}} \quad \equiv \text{Thermal Utilization Factor}$$

$$p \quad \equiv \text{Resonance Escape Probability}$$

$$\epsilon = \frac{TotalFission(n)}{ThermalFission(n)} \quad \equiv \text{Fast Fission Factor}$$

To define a few more terms, the Thermal Utilization factor is the fraction neutrons that are absorbed by the fuel of the core, the Resonance Escape Probability is the fraction of fission neutrons that manage to slow down from fast to thermal energies without being absorbed, and the fast fission factor is the fraction of neutrons generated by fissions caused by fast neutrons. From the four factor formula, equation (2.2), it is clear that the criticality of a system is both material and geometry dependent, leading

to more decisions in the design process with respect to what level of k_{eff} we wanted to operate at. While some reactors are able to operate at a critical state or operate in a pulsed fashion, we decided that, for the amount of ^{99}Mo we wanted to produce, our reactor would need to be subcritical, and stay below a critical operation level ($k_{eff} = 1$) at all times. Hence, additional neutrons will be needed as opposed to a sustained reaction. Subcriticality therefore defined the means of our fuel choice and geometry of the core given the nature of determining k_{eff} .

2.2 Molybdenum-99 Production via Reactions

There was also the case of how we wanted to produce the ^{99}Mo in the system. There are a variety of different ways to produce ^{99}Mo on large-scale, so the decision of which way the production occurred was crucial. Table 2.1 shows the various ways in which ^{99}Mo might be produced.

Nuclear Reaction	Cross Section	Yield
Natural $^{98}\text{Mo}(n,\gamma)^{99}\text{Mo}$	0.13b	2 Ci $^{99}\text{Mo}/\text{g Mo}$
Enriched $^{98}\text{Mo}(n,\gamma)^{99}\text{Mo}$	0.13b	10 Ci $^{99}\text{Mo}/\text{g Mo}$
$^{100}\text{Mo}(\gamma, n)^{99}\text{Mo}$	100kW e^- beam	1,079 Ci, 3.9 Ci $^{99}\text{Mo}/\text{g Mo}$
$^{235}\text{U}(n,f)^{99}\text{Mo}$	586b (6.11%)	> 10,000 Ci $^{99}\text{Mo}/\text{g Mo}$
$^{239}\text{Pu}(n,f)^{99}\text{Mo}$	747.4b (6.21%)	> 10,000 Ci $^{99}\text{Mo}/\text{g Mo}$

Table 2.1: The relative ^{99}Mo yield from varying nuclear reactions

There were a few fuel sources that were very quickly disregarded. While Plutonium-

239 would likely produce the necessary amounts needed to meet our design's production demands, there are some non-technical issues surrounding it. Presently, there are many civilian restrictions on the use and handling of Plutonium, thus severely limiting the individuals who might be able to work in the facility. Additionally, the construction of a reactor using Plutonium for the sole purpose of producing a single radio-isotope would likely draw criticism from the surrounding neighborhoods and governments with regards to economic strains from taxpayer dollars, and general perception of nuclear safety. A number of isotopes of Molybdenum were also considered, but ultimately rejected as possible fuel sources. Both natural and enriched ^{98}Mo would likely be safe to use, but not meet the design requirements. Using ^{100}Mo as the fuel source would also be problematic as it not be likely to yield the proper amount of ^{99}Mo necessary for our design specifications, and furthermore would produce a 100kW electron beam yielding approximately 1,100 Ci. Therefore, these sources were thrown out in favor of using fission products from Uranium-235.

2.3 Material Decisions

Because of the choice to use LEU targets, there were some material decisions that had to be kept in mind during both the initial design process and the proceeding evolutionary steps. From existing references like the reactor at SHINE, it was clear that the core would need some kind of shielding with water acting as a moderator, as well as a neutron shield. The water surrounding the core, therefore, was a simple choice for our design, as it would also be helpful in cooling the core as well. For the barrier surrounding

the water, concrete was chosen for its ability to shield thermal neutrons.

2.4 Accelerator Information

Given the nature of our project being centralized in Madison, Wisconsin, it would make sense to use locally sourced technologies to construct our reactor. Phoenix, a neutron generator manufacturer stationed out of Monona, WI, has an accelerator design that matches up very well for the technical specifications of our design. The Alectryon design was selected for this project due to the fact that it “is the highest yielding deuterium-tritium (DT) compact neutron generator in the world” [7], with source strengths ranging from 1×10^{13} to 5×10^{13} DT n/s when used with tritium fuel. Even at its lower boundary, the source strength for a higher neutron yield is appropriate for the context of this design given that the design aims to produce a large quantity of medical isotopes.

2.5 Design Refinements

While the concept was consistently a convection-cooled subcritical reactor using LEU targets as fuel, there were many structural and geometry developments that took place over the course of the design process. Initially, we wanted to explore the differences between a homogeneous solution and a target based system. The main core design followed a very straight-forward, and rather basic, design, with a simple homogeneous solution in order to benchmark a critically. After the criticality was benchmarked around

0.99, the core was then discretized in such a way in order to insert circular targets into a hexagonal lattice as shown in Figures 2.1. The hexagonal lattice scheme proved to be effective in producing a proper criticality, but was decided to be a little too difficult for target manufacturing and arrangement in the core. Therefore, the shape of the lattice was converted from hexagonal to square. While this change did end up causing significant geometry changes with the dimensions of the core, it ultimately proved to be much easier to optimize target placement and critically control. From this point, the positioning of the targets was altered on a case-by-case basis in order to find the most effective layout of targets. An early potential schematic can be seen in Figure 2.2. From this point, the core geometry was altered and adjusted in order to maintain a $k_{eff} < 0.99$. The material in the core including the LEU enrichment and Zirconium cladding among other material properties, as previously noted, were kept fairly constant in order to not overcomplicate the analysis of the core geometry.

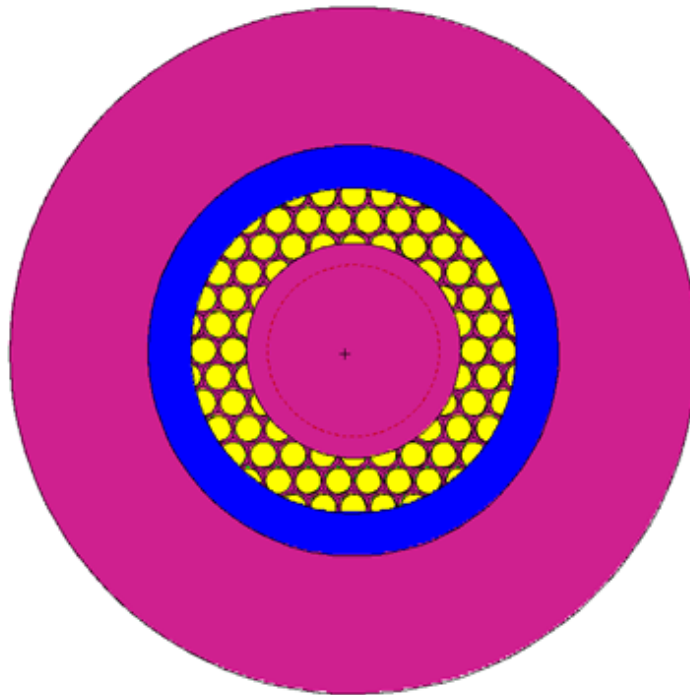


Figure 2.1: Top-down view of the hexagonal lattice scheme

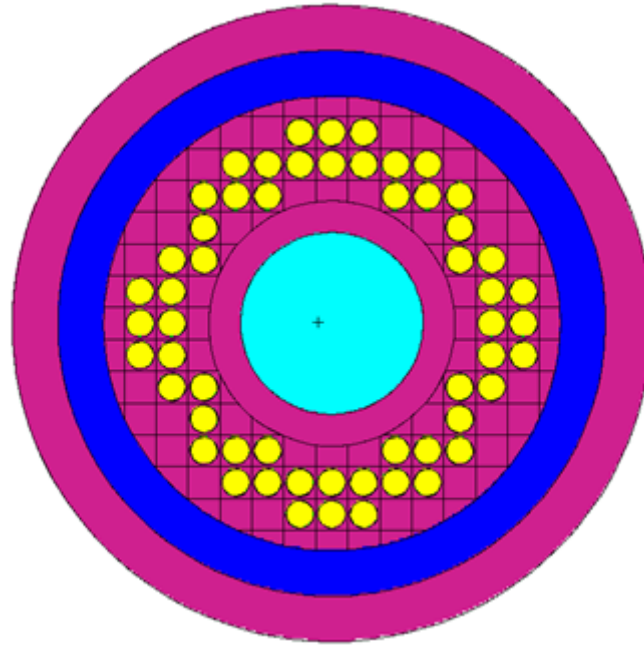


Figure 2.2: Top-down view of an initial target distribution in a square scheme

2.6 Design and Project Limitations

As with all senior design projects, there are limitations to our design, which we lay out now. These limitations vary in minor technical issues to significant design constraints.

The primary limitation on this design comes from the nature of the project as a whole. This project is developed from scratch to a result in the span of four months amongst three people. It is likely given far more time and resources, this project would be a much more refined system. Furthermore, with the COVID-19 pandemic becoming a significant global issue halfway through the project, which prevented in-person gatherings, there were notable limitations on access to software and resources normally available for students working on their senior designs.

Additionally, there is also the fact that in order to truly know if a design is functional and effective, it needs to actually be built. This project lacks any sort of funding that would allow for the purchase of an accelerator, targets or any other aspect of the design. While we can assume that the computational results obtained from MCNP6 are accurate and realistic, there is presently no way to verify that the design is truly functional. This also begs the question of where exactly a facility of this nature would be built in the city of Madison. While there is a large greenspace near the UW Hospital, the construction clearances and costs would ultimately prove to be very difficult to realistically manage. The location of an adequate construction site is something that might be solved with more time and resources, though the actual construction would likely be something that would require far more time, money and energy than is realistic for a senior design project. The economics of this project as a whole will be discussed further along in the report.

2.7 Design Parameters

The design summary table is given below.

Table 2.2: Design Summary Table

Thermal Output [kW]	4.408
Peak Power Density [W/cm ³]	0.324
Average assembly Power Density [W/cm ³]	0.004521
Peak Fuel Temperature [°C]	28.414
Fuel Material	UO ₂
Fuel Enrichment	19.75%
Fuel Cladding	Zircaloy 4
Coolant	Light Water
Moderator	Light Water
Emergency Poison	Gadolinium Nitrate
Target Assembly Lattice	Square
Target Shape	Cylindrical
Number of Targets	60
²³⁵ U fissions/s	1.29×10^{14}
²³⁸ U fissions/s	6.15×10^{12}
Final ⁹⁹ Mo Activity at the end of batch [Bq]	2.51×10^{18}
Final 6-day Curies produced per batch	36.7
²³⁹ Pu produced per batch [mg]	4.53
Maximum DPA/s in target gridbox	1.52×10^{-11}

Chapter 3

Molybdenum-99 Production Process

3.1 Duty Cycle

One of the most important parts of this project has been to develop an appropriate timeline in which the ^{99}Mo produced is optimized. Outlined below is each step in its entirety, beginning with the production of the targets and ending with the shipment of the ^{99}Mo . The duty cycles will undergo stages in the order which they are actually to take place: target production, irradiation, cooling, chemical treatment, and then finally transportation. The rate equation governs how much ^{99}Mo will be at the end of the duty cycle. Therefore, the rate equation governs if we reach our design goal of a minimum of 450 6-day curies. In the end, the design reaches 37 6-day curies, well below our target.

3.2 Target Production and Irradiation Process

The targets will be bought from one of the three Low-Enriched Uranium Fuel Fabrication Facilities that are approved by the NRC in the US that already produced UO_2 [8]. During this purchase, the design specifications will be provided to the companies for an adequate delivery of the needed shape of the pins. Without a proper scaling and sizing of the fuel pins, the system could fail in a variety of different ways, so it is crucial that the fuel sources are manufactured properly. Next, the targets are placed into the assembly and then irradiated for 6 days, as outlined in Table 2.2, the Design Parameters.

3.3 Cooling Stage

Once irradiated, targets are cooled for approximately one hour. The cooling process occurs simply by powering down the accelerator and moving the fuel pins to the storage pit in the same pool of water and allowing the pool of water, already in place, to remove heat via convection. The relatively low temperatures reached in our core, only reaching a peak heating of approximately 4.4 kW, allows for a quick cooling process. This transfer process is time-consuming and the storage of the fuel pins in the cooling pit is essentially an intermediate step. After this cooling period, each pin is again removed one at a time and transported in shielded casks to the in-house chemical processing facility.

3.4 Chemical Treatment

The targets are transferred to hot cells, similar to that seen in Figure 3.1 and 3.2 [9]. Processing is done relatively quickly because about 1 percent of the Mo-99 produced in the target is lost to radioactive decay every hour after irradiation. Therefore, processing only take about one to two hours to complete. With an Uranium Oxide target, an acid dissolution process will be used as opposed to an Alkaline dissolution process.

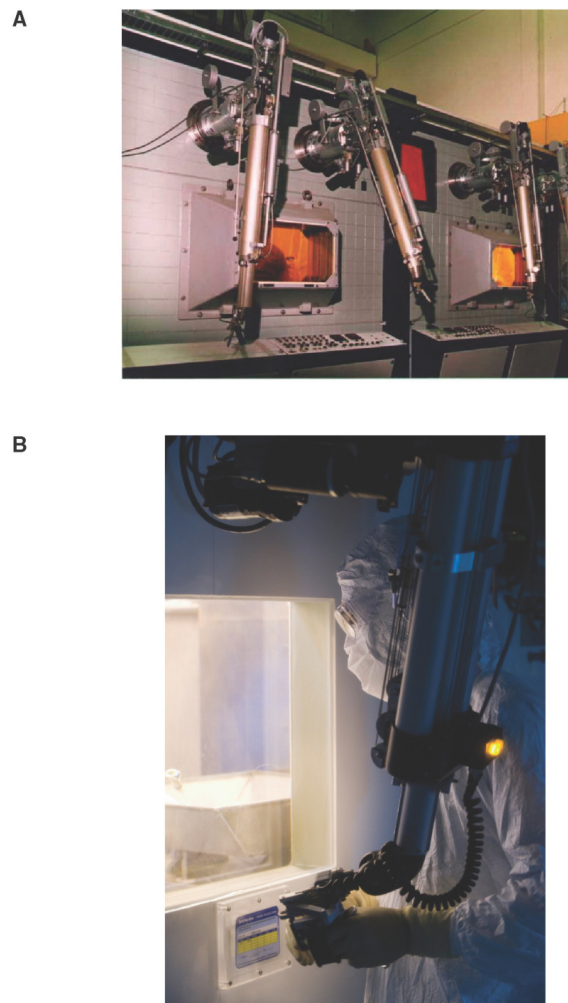


Figure 3.1: Hot Cells in use for processing Mo-99 from an LEU source. [9]

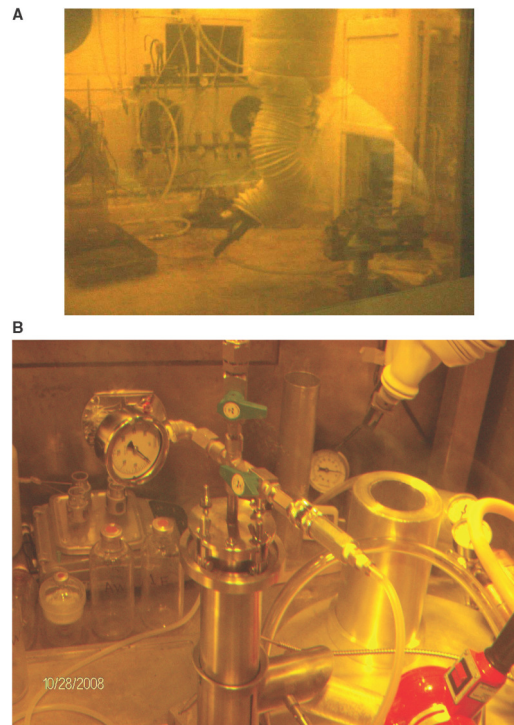


Figure 3.2: (a) a view into the Hot Cell and (b) a view of the dissolving agents used in the chemical treatment process [9]

In the process, the Uranium part of the target is physically separated or leached from the cladding and then dissolved in nitric acid. This leads to a formation of a Nitrate solution (NO_3^-) containing Uranium, Molybdenum, and all other fission products besides volatile gases (i.e. Iodine, Xenon, Krypton, etc.). Next, to recover pure Molybdenum, the solution is placed in an ion exchange resin. Then, the Molybdenum is washed with an appropriate solution to remove any residual fission products or Uranium. The acid dissolution process has a ^{99}Mo recovery yield which exceeds 85-90 percent (includes loss from time of extraction). The waste from the removed cladding and the liquid solutions can be stored in tanks or mixed with cement to immobilize it.

3.5 Transportation Methods

Transportation of the pins to the processing facility will be in shielded casks. After processing, the waste from the removed cladding and the liquid solutions can be stored in tanks or mixed with cement to immobilize it. The separated ^{99}Mo is then transported in shielded casks to the respective hospitals. The casks used will follow the US N.R.C. and Department of Transportation guidelines as outlined in their reports [10].

3.6 Summary and Rate Equation

From these steps, we developed a rate equation that models the process of the production rates of Molybdenum-99, (Mo).

$$\frac{\partial Mo}{\partial t} = \gamma_{Mo} \Sigma_{Mo,f} \phi(r, t) - \lambda_{Mo} Mo(r, t) - \Sigma_{Mo(n,\gamma)} \phi(r, t) \quad (3.1)$$

where

$\Sigma_{Mo,f}$	\equiv The fission cross-section for ^{99}Mo
$\Sigma_{Mo(n,\gamma)}$	\equiv The fission neutron-capture cross sections for ^{99}Mo
λ_{Mo}	\equiv The half life of ^{99}Mo
$\phi(r, t)$	\equiv The time-dependent flux

However, given the nature of the (n, γ) cross section being significantly small, it can be considered negligible in this case. The differential equation can be approximately solved with an integrating factor, while also considering where in the production process

there would be increases or decreases of activity, to get the equation that models the total amount of ^{99}Mo . This modelling equation which is shown below in equation (3.2):

$$N_{99\text{Mo}} \approx \frac{\gamma_{\text{Mo}} \Sigma_f \phi(r, t_{\text{irr}})}{\lambda_{\text{Mo}}} (1 - e^{-\lambda_{\text{Mo}} t_{\text{irr}}}) \times e^{-\lambda_{\text{Mo}}(t_{\text{cool}} + t_{\text{transfer}})} \times \epsilon \quad (3.2)$$

where

t_{irr}	\equiv	The time the targets are irradiated
t_{cool}	\equiv	the time spent in the cooling pools
t_{transfer}	\equiv	The being transferred from location to location, respectively
ϵ	\equiv	The process efficiency

Naively, the first term in equation (3.2) would be the total amount of ^{99}Mo produced in a given irradiation period assuming absolutely no losses from decay or process efficiency. As previously noted, the maximum time for transportation is assumed to be approximately an hour, and the time in which the products are cooling in the pool is approximately one hour. With the applied constants be substituted into the equation and running the simulations in MCNP, the rate equation calculations lead to a design that will produce 37 6-day curies per duty cycle, well below the goal of a minimum of 450 6-day curies.

Chapter 4

Neutronic Analysis

MCNP6, a Monte Carlo computer code, was used to perform neutronics calculations for the target assembly design and guided the design process as the semester went along. The primary goal of the neutronics analysis was to determine which geometry and enrichment configurations allowed for the highest production of ^{99}Mo while still remaining subcritical. The neutronics analysis ultimately showed that the maximum LEU enrichment was beneficial towards maximizing ^{99}Mo production while reducing the amount of ^{239}Pu produced in neutron capture by ^{238}U . After finalizing this base geometry, details were added to the assembly, and other important MCNP calculations were conducted for use in the shielding, thermal, and safety analysis of the report.

4.1 Hand Calculations

Before running any neutronics calculations in MCNP, hand calculations were used in order to give a rough estimate of the size and desired characteristics of the target

assembly. While the final design calls for a target based approach, a homogeneous cylindrical reactor model was first used to simplify the calculation and provide the dimensions to be used for our initial MCNP input file.

In order to begin calculations, a target composition needed to be determined. There were many different options available to choose from including uranium-aluminide (UAl_4), uranium-silicide (USi_2), uranium nitride (U_2N_3), uranium foil, and uranium oxide (UO_2) targets. These compounds have all been researched or used for irradiation in research reactors, so therefore, the choice of target material ultimately affected the density of the targets, as well as the chemical process utilized to separate the ^{99}Mo product. Initially we decided to use higher density targets to increase the neutron flux and allow for tighter packing around the accelerator neutron source, though section 4.6 of the report describes why a high uranium density may not have been the best selection for our subcritical reactor design. The two highest density target types are uranium foils with a density of 19.0 g/cm^3 and UO_2 with a 9.7 g/cm^3 density. Uranium foil targets have yet to see commercial use in large scale production of ^{99}Mo , so a UO_2 target composition was selected [11].

With the fuel type selected, the one-speed diffusion model for nuclear reactors was used to perform the initial criticality calculation for the homogeneous reactor. While the ultimate goal for the system is to remain subcritical, it was important to have the assembly be as close to critical as possible (limited by the factor of safety desired) in order to maximize the yield of ^{99}Mo being produced. Therefore, a critical reactor will give a close overestimation of the size of the subcritical homogeneous assembly. The criticality condition in the one-speed diffusion model requires geometric buckling to be equal to

material buckling.

Material buckling is dependent on the material composition of the reactor fuel. This is the parameter we set to a fixed value as the desired 19.75% enrichment and UO_2 composition of the fuel were already selected for the assembly design. Material buckling can be calculated using equation (4.1).

$$B_m^2 = \frac{\nu\Sigma_f - \Sigma_a}{D} \quad (4.1)$$

where

B_m \equiv The material buckling value

ν \equiv Average number of neutrons produced per fission (for ^{235}U this is 2.43)

Σ_f \equiv Macroscopic fission cross-section of fuel

Σ_a \equiv Macroscopic absorption cross-section of fuel

D \equiv Diffusion length

The diffusion length describes the mean square distance a neutron travels in one direction before absorption. This is a material dependent value that is calculated using equation (4.2).

$$D = \frac{1}{3(\Sigma_t - \mu_0\Sigma_s)} \quad (4.2)$$

where

- Σ_t \equiv The total macroscopic cross-section
 μ_0 \equiv Diffusion constant
 Σ_s \equiv Macroscopic scattering cross section of fuel

Once the material buckling value was determined, the dimensions of the cylinder necessary to achieve criticality could be decided. This is done by setting the material buckling equal to the geometric buckling in equation (4.3).

$$B_m^2 = B_g^2 \quad (4.3)$$

where B_g^2 is the geometric buckling value. The geometric buckling for a finite cylinder depends on the height and radius of the cylinder seen in equation (4.4).

$$B_g^2 = \left(\frac{\nu_0}{\tilde{R}} \right)^2 + \left(\frac{\pi}{\tilde{H}} \right)^2 \quad (4.4)$$

where,

- ν_0 \equiv The first zero of the Bessel function of the first kind (=2.405)
 \tilde{R} \equiv The extrapolated cylinder radius ($\tilde{R} = R + z_0$)
 \tilde{H} \equiv The extrapolated cylinder radius ($\tilde{H} = H + z_0$)
 z_0 \equiv The extrapolated length

The extrapolation length describes the distance from the end of the reactor that the neutron flux drops off to 0. For the purposes of the baseline we set the core height to be 100 cm, as that is the height of the neutron accelerator used as the neutron source

in this system. This resulted in an initial radial guess for a 19.75% enriched UO_2 reactor of 12.3 cm.

4.2 Initial Homogeneous Reactors

A bare homogeneous reactor was modeled in MCNP to get a very general idea of the dimensions of the reactor, and to familiarize ourselves with MCNP. To make the calculation a little more relevant to the eventual design, water was added to the homogeneous reactor. An arbitrary atom ratio of two water molecules for every UO_2 molecule in the mixture was decided upon. By maintaining a fixed cylinder height of 100 cm, the radius was changed until the reactor was near exactly critical. Table 4.1 shows the characteristics of the homogeneous reactor modeled.

Atom Ratio of UO_2 and H_2O	Mixture density [g/cm^3]	Reactor height [cm]	Reactor radius [cm]	k_{eff}
2:1	8.7	100	9.3	1.00758

Table 4.1: Homogeneous UO_2 and H_2O reactor characteristics

To improve upon the design of the homogeneous reactor, the core was changed to a tube shape and dehomogenized. The tube shape provides room to insert the Alectryon neutron accelerator which would drive the subcritical multiplication in the target assembly. An arbitrary inner radius of the UO_2 fuel was selected to be 12.5 cm to fit the 10 cm radius of the neutron source. Criticality calculations were run again with water inside the tube to determine the dimensions needed to make such a bare reactor critical. Table 4.2 shows the characteristics of the updated simple reactor.

H₂O density [g/cm ³]	UO₂ density [g/cm ³]	Core Height [cm]	Inner Radius [cm]	Outer radius [cm]	k_{eff}
1	9.7	100	12.5	18	1.00758

Table 4.2: Simple Tube reactor characteristics

The initial calculations suggested the height of the subcritical assembly would be in the tens of centimeters, and the width be on the order of centimeters. The sizes shown in the previous two tables are gross over estimations as the code immediately terminated any neutrons that left the reactor. The addition of reflectors and improved moderation also contributed towards shrinking the subcritical target assembly.

4.3 Accelerator Source Modelling

As previously noted in the accelerator specifications section of Chapter 2, subcritical multiplication in the target assembly is driven by Phoenix's Alectryon neutron accelerator. Phoenix lists the source strength of the accelerator to be between 1×10^{13} and 5×10^{13} DT n/s, therefore the 1×10^{13} n/s source strength was used in our model to provide a conservative estimate of the assembly's ⁹⁹Mo production capability. The generator works by accelerating ionized deuterium towards a tritium gas target, so if operating under the proper conditions, deuterium tritium fusion takes place within the chamber. Equation (4.5) shows the reactants and products of the reaction.



Where Q is the energy released from the system. In this case, 14.1 MeV neutrons produced in this reaction were isotropically scattered, which was easily handled in MCNP.

Given the lack of information provided by Phoenix on their website, proper modeling of the geometry and reaction location within the chamber of the Alectryon accelerator was next to impossible. Discussions with Professors Murphy and Bohm resulted in the decision to create an approximate accelerator with a height of 100 cm and radius of 10 cm. These dimensions set the boundaries for where neutron particles could be born. However, no data could be found to understand the concentration of fusion reactions as a function axial and radial position within the tritium chamber. Our model approximated a uniform distribution within the cell modeling the accelerator. This is likely an incorrect assumption, as deuterium energy is likely decreasing as it travels through the tritium gas while also diffusing radially outwards from the initial ion beam. An uneven source distribution could be taken advantage of if such a distribution is well understood. Targets could be placed around regions containing the highest D-T fusion density to improve source neutron utilization. Due to the lack of knowledge, a uniformly distributed neutron source position was assumed in order to provide a conservative approximation to our model.

4.4 Detail and Sizing Progression

Following the completion of general sizing calculations, additional details were added to the subcritical system in steps. The tube shaped slab of UO_2 was split into fuel pins with Zircaloy-4 cladding. Zirconium-based cladding was selected for this design due to its low neutron absorption cross section and widespread use in commercial power

reactors. Any potential accident scenarios experienced by the cladding in our subcritical assembly pale in comparison to the corrosion and temperature stressed Zr cladding experiences in critical reactor usage. Graphite reflectors were added to both ends of the cylindrical fuel element to smooth out the axial flux profile. The target pins were then placed in a square lattice around the accelerator source. As previously noted in the initial design evolution section of Chapter 2, some consideration was given towards the use of a hexagonal lattice to potentially smooth out the flux profile. While this geometry was considered for a short period, the square lattice was ultimately decided upon as ease of manufacturing was favored in the end. Lastly, a circular graphite reflector was added around the lattice to maintain the neutron population within the target region.

We then tested two different design ideologies to determine which method should be followed to the finalized design. An assembly with lower 12% enrichment, but larger target size was compared against a smaller 19.75% enriched target. The theory behind the low enrichment was that more source neutrons would be used to drive subcritical multiplication while the higher enrichment plan was to maximize the utilization of fission neutrons by having a more tightly packed geometry. The geometries were made to have nearly identical multiplication factors to allow for equal comparison. When the geometries were sized correctly, a fission rate calculation was conducted to compare their Mo-99 production capabilities. Table 4.3 shows the design parameters of the low vs high enriched assemblies.

Design Methodology	Lower Enrichment	Higher Enrichment
Target Enrichment [%]	12	19.75
UO ₂ length in target [cm]	60	45
k_{eff}	0.984	0.985
Total Fission rate [1/s] ¹	1.20×10^{16}	3.52×10^{16}

Table 4.3: Homogeneous UO₂ and H₂O reactor characteristics

From the data presented in the table, the 19.75% enriched target assembly proved to be better suited towards producing ⁹⁹Mo. This was a welcome observation as higher enriched targets are also known to produce less ²³⁹Pu waste through neutron capture of ²³⁸U.

Following the decision to remain with 19.75% enriched uranium, fewer neutronics based additions were added to the geometry, and instead there were more. A target grid box made of AISI 1335 steel was added to support and lock the targets into place during irradiation. This steel, which is primarily made of iron, manganese, and phosphorus, was selected due to its low activation properties. Low activation is favorable in the event any repairs need to be done on the target gridbox and reduce waste activity when the decommissioning of the facility inevitably occurs. Figure Figure 4.1 describes each element's activation tendencies for slow and fast fluxes and was used to select an ideal steel alloy [12]. Elements in green are lower activation hazards compared to all other elements.

¹NOTE: fission rates were scored using an incorrect tally technique. Results are incorrect but can still be used to identify the improved production rate for higher enrichment targets

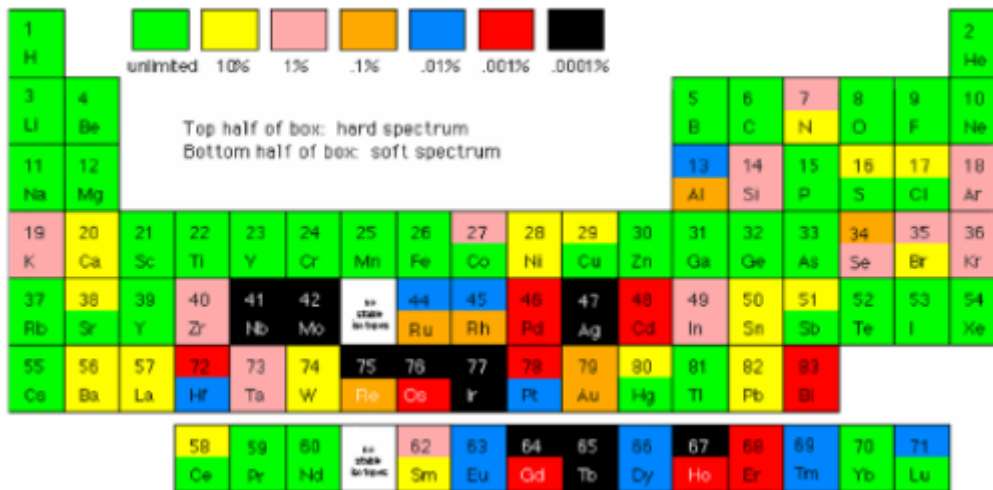


Figure 4.1: Table presenting activation risks of different elements

To reduce heating in the target pins, the pitch of the lattice was increased from 3.5 cm to 3.8 cm. 0.7 cm radius coolant channels were added to the grid box to improve coolant circulation.

A stainless steel fitting was added to the bottom of the target to guide the targets into the gridbox. A stainless steel ring was added to the top of the fuel pin to allow workers to latch on the targets and load and unload the targets to the core, storage pit, and ultimately the hot cell.

4.4.1 Finalized Assembly Geometry

This section provides basic MCNP schematics and tables describing the final geometry of the subcritical target assembly. The k_{eff} for the final design is 0.9867.

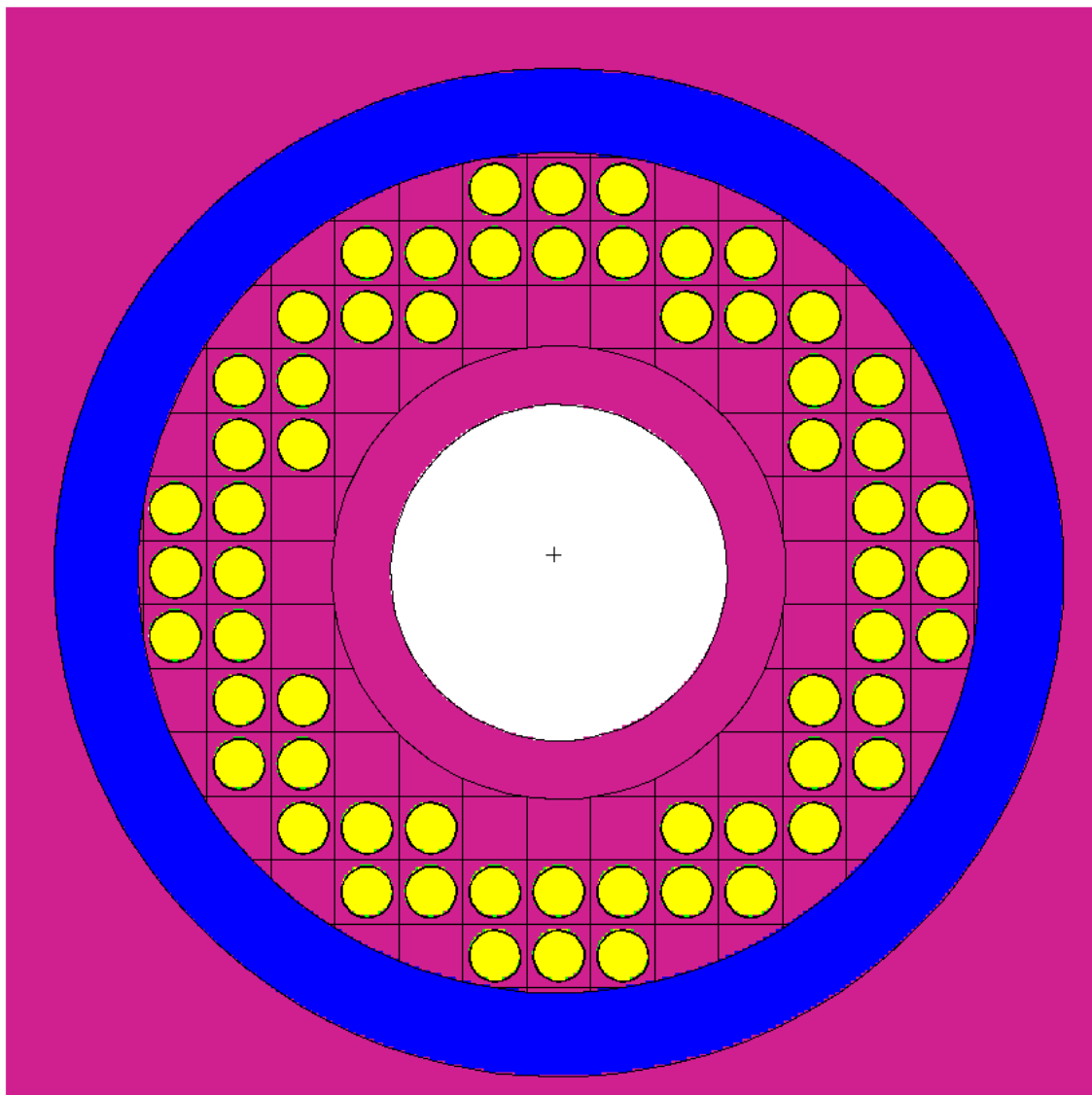


Figure 4.2: Top down view of the assembly

Accelerator radius [cm]	10
Grid box inner radius [cm]	13.5
Grid box outer radius [cm]	25
Reflector inner radius [cm]	25
Reflector outer radius [cm]	30
Number of targets [-]	60
Diameter of targets [cm]	3.102
Target pitch [cm]	3.8
Pitch to diameter	1.22502

Table 4.4: Homogeneous UO_2 and H_2O reactor characteristics

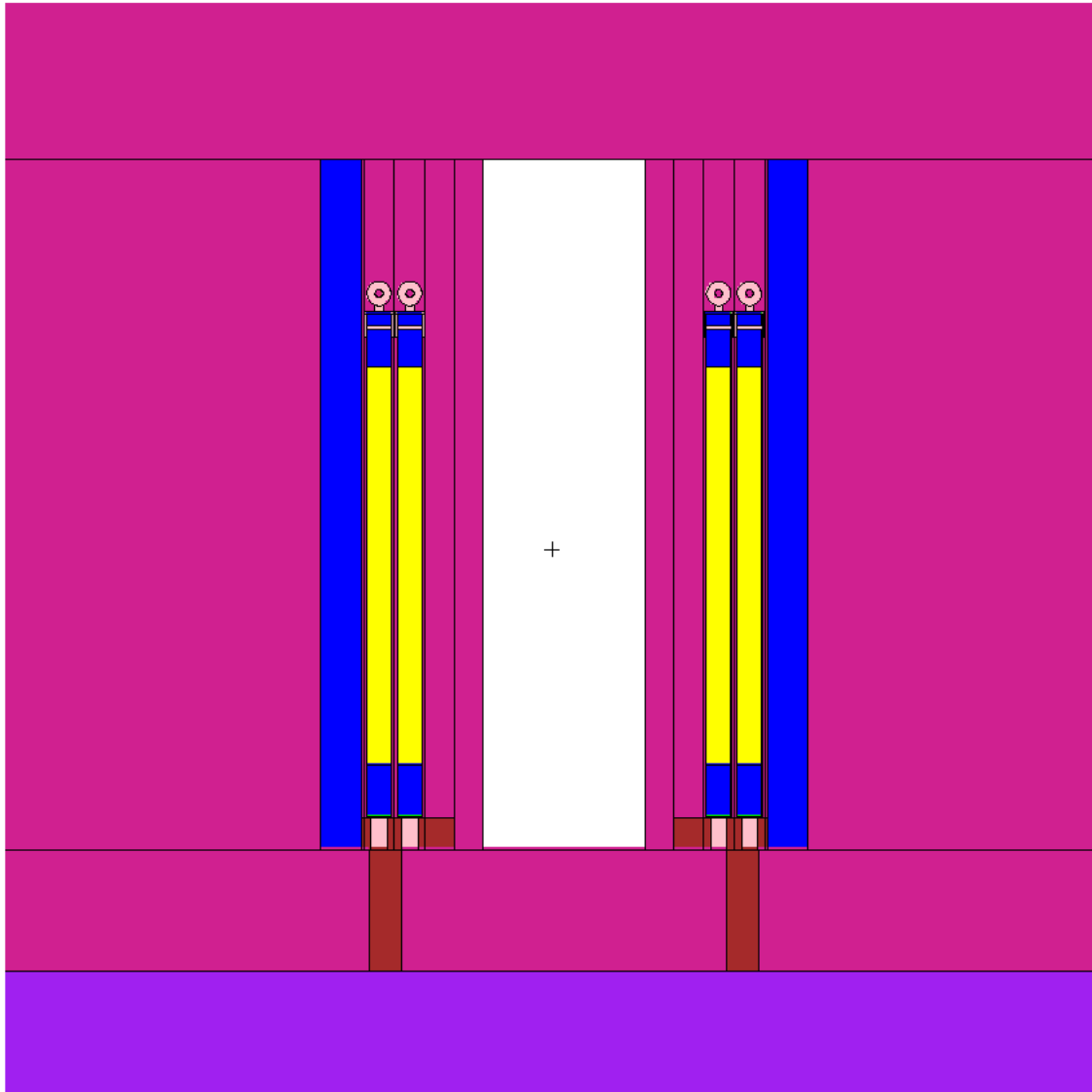


Figure 4.3: Side view of the assembly

Accelerator chamber height [cm]	100
Outer reflector height [cm]	85.0508
Grid box outer radius [cm]	4
Number of legs holding gridbox [-]	8
Leg height [cm]	14.9492
Number of targets [cm × cm]	4 × 4

Table 4.5: Homogeneous UO_2 and H_2O reactor characteristics

¹NOTE: It must be noted that the geometry plotted directly below the source container is inaccurate. This space would actually be taken up by the deuterium ion beam and other components of the neutron accelerator.



Figure 4.4: Side view of individual targets

UO ₂ region length [cm]	49
UO ₂ region radius [cm]	1.5
Graphite reflector length [cm]	6.5
Zircaloy 4 cladding thickness [cm]	0.0508
Stainless steel bottom fitting length [cm]	4
SS bottom fitting thickness [cm × cm]	2 × 42
SS top fitting inner radius [cm]	1
Total target length [cm]	73.0508

Table 4.6: Key dimensions of target

4.5 Flux Profile

Neutron flux profiles were plotted to get a better understanding of the flux profile within the subcritical system. Figures 4.5 and 4.6 show the MCNP flux plots generated using a mesh tally.

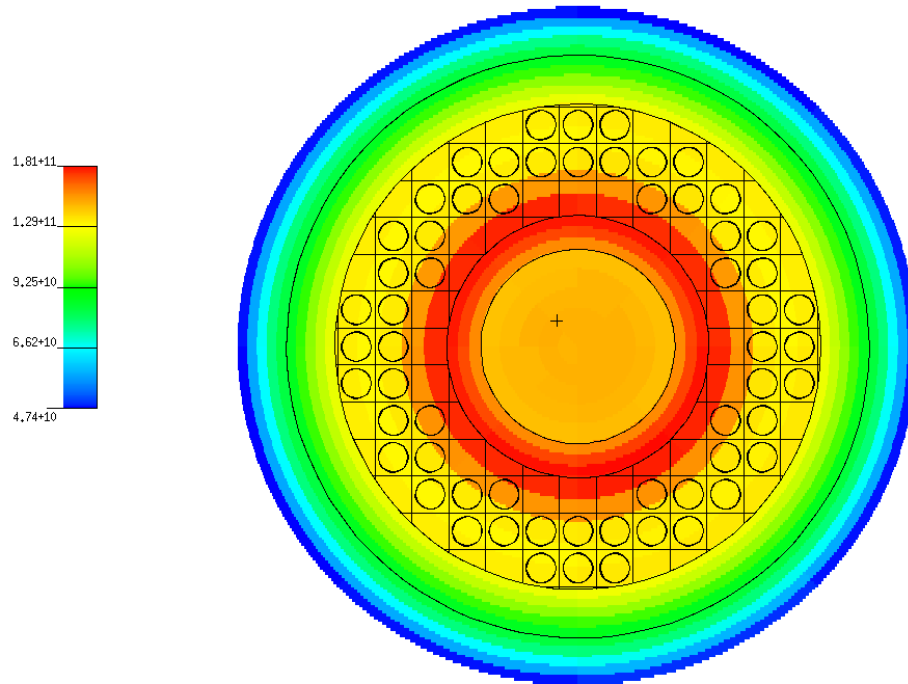


Figure 4.5: Neutron flux as function of radial position plotted over assembly geometry

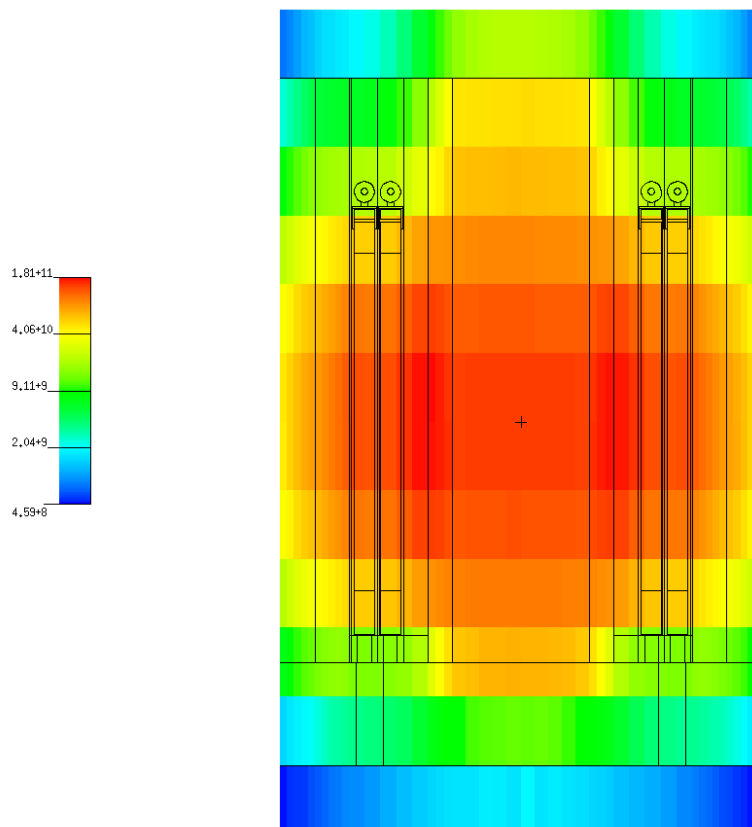


Figure 4.6: Flux profile plotted over side view of assembly to show axial dependence of neutron flux

Unfortunately, the MCNP plots are busy and difficult to follow. To get a better understanding of the flux profile, 2-D plots showing the radial dependence of the flux profile are provided in figures 4.7 and 4.8. Figure 4.8 divides neutron flux into three distinct energy regimes: the thermal bin (containing neutrons with an energy of 0.625 eV and below), the epithermal bin (containing neutrons ranging from 0.625 eV to 0.1 MeV) and the fast bin (neutrons with energies over 0.1 MeV).

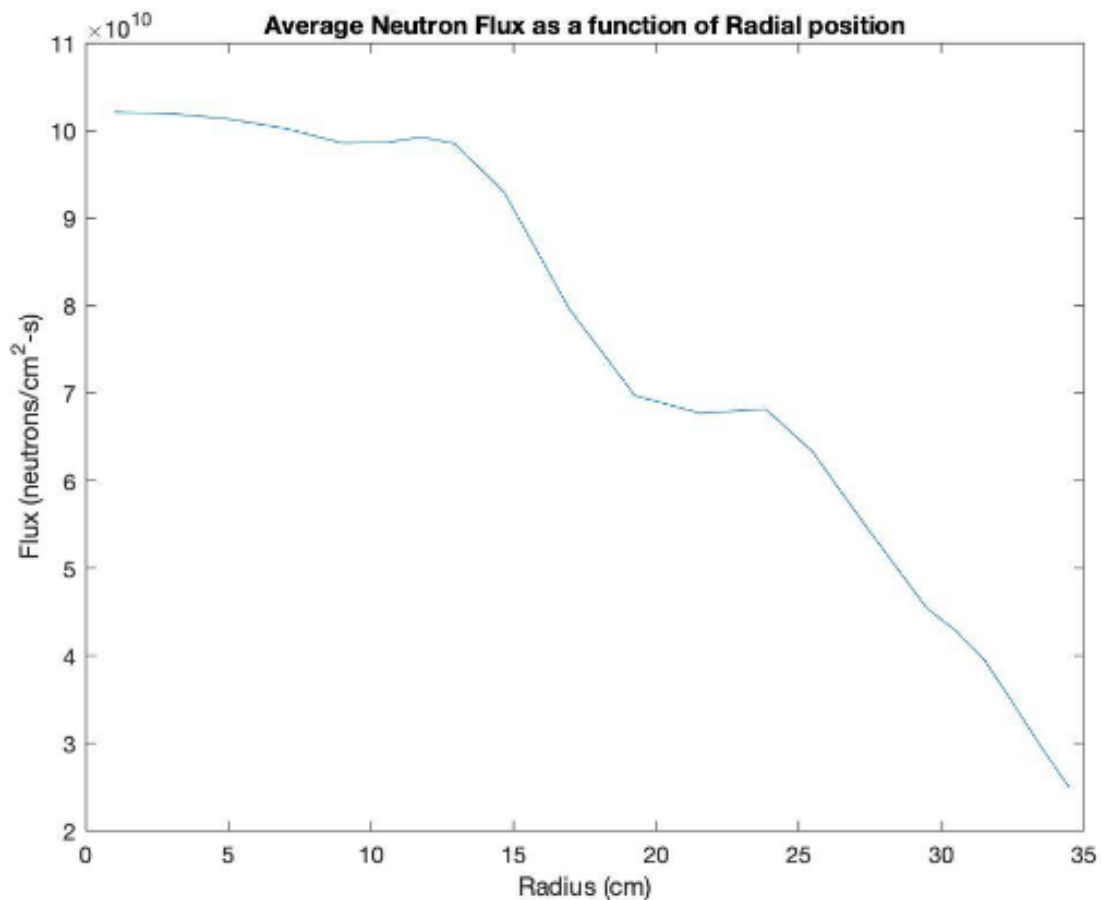


Figure 4.7: Neutron flux as a function of radial position in assembly

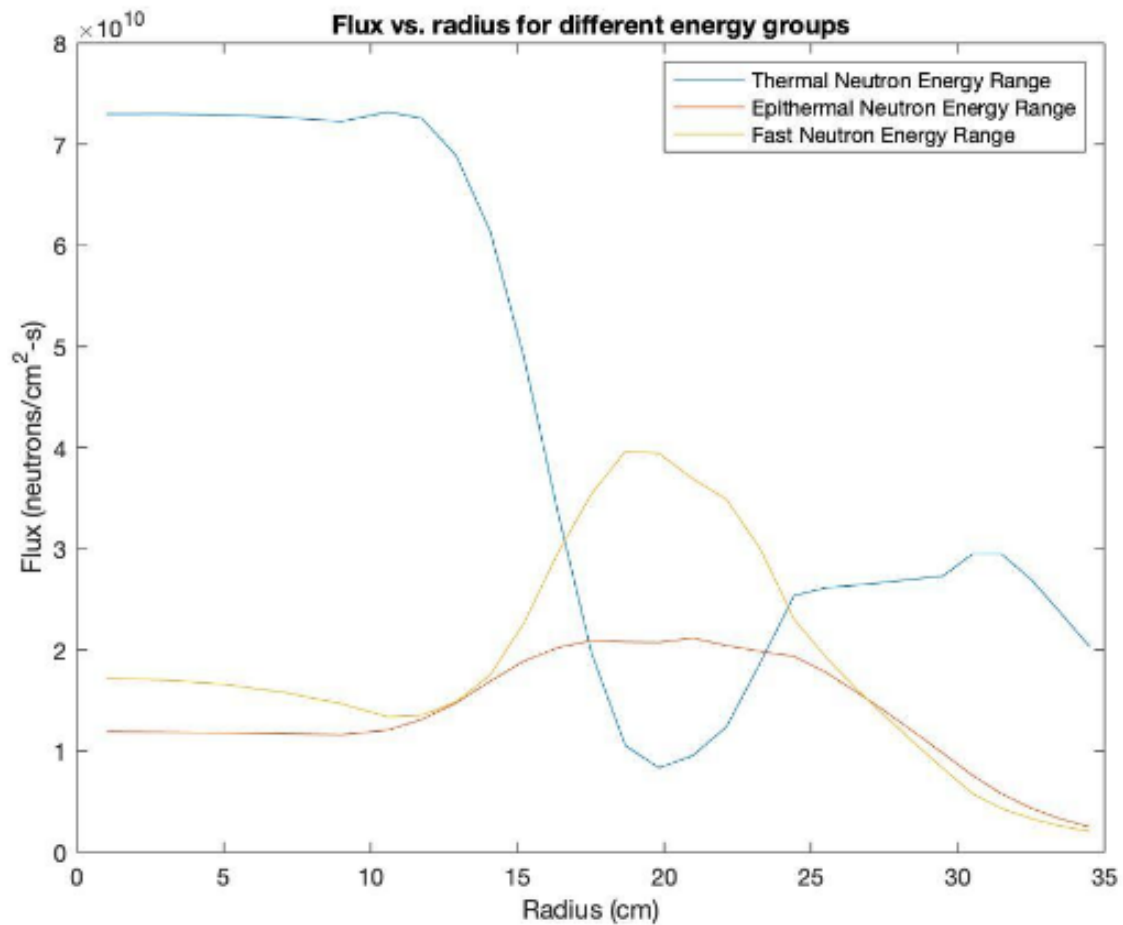


Figure 4.8: Neutron flux as a function of radial position in the assembly divided into three energy groups

Figure 4.7 behaves as expected. The flux profile drops are similar to a cosine shape with bumps in regions where the targets are located. Figure 4.8 gives a more detailed view of the flux profile in the assembly. It is interesting to see how quickly the thermal flux profile drops when entering the target region. The drop is offset by a spike in fast and epithermal neutrons through thermal fission in the UO_2 target.

4.6 Final ^{99}Mo Production

^{99}Mo production in the assembly was calculated by tracking the fissions/s of both ^{235}U and ^{238}U in each target pin. Table 4.7 summarizes the findings of the fission tallies:

Isotope	^{235}U	^{238}U
Average Fission Rate Pin [fission/sec]	2.309×10^{12}	1.026×10^{11}
Maximum Fission Rate Pin [fission/sec]	2.966×10^{12}	1.154×10^{11}
Minimum Fission Rate Pin [fission/sec]	1.745×10^{12}	9.021×10^{10}
Fission Rate Coefficient of Variation [%]	13.12	6.612
Total Fission Rate of Assembly [fission/sec]	1.386×10^{14}	1.026×10^{11}

Table 4.7: Key dimensions of target

One notable thing from this table is the significantly larger coefficient of variation for ^{235}U fission rates in each pin versus that of ^{238}U . The coefficient of variation is a measure of the spread of data, and is calculated by dividing the standard deviation by the mean of a data set. The larger coefficient of variation suggests a much flatter fast neutron flux profile over the targets compared to the thermal profile. A fast fission factor for the subcritical reactor was approximated to be 1.051 by taking the ratio of ^{235}U and ^{238}U fission rates and using equation (4.5) [13]. The higher fast fission factor of 1.051 compared to typical thermal reactors 1.02-1.03 is expected due the use of the 14.1 MeV neutron source driving subcritical multiplication. Equation 3 assumes all of the ^{235}U fissions happen at thermal energies and that all of the ^{238}U fissions occur at fast energies.

$$\varepsilon = \frac{\nu_p(^{235}\text{U})F + \nu_p(^{238}\text{U})}{\nu_p(^{235}\text{U})F} \quad (4.6)$$

where

$$\begin{aligned} \nu_p(^{235}\text{U}) &\equiv \text{The prompt neutron yield of } ^{235}\text{U} (=2.419) \\ \nu_p(^{238}\text{U}) &\equiv \text{The prompt neutron yield of } ^{238}\text{U} (=2.773) \\ F &\equiv ^{235}\text{U fission rate} / ^{238}\text{U fission rate} \end{aligned}$$

The thermal fission yields for ^{235}U and the fast fission yields for ^{238}U are both slightly energy dependent and not identical. However, figure 4.9 shows that the ^{99}Mo fission yield for ^{235}U and ^{238}U and for the purposes of this analysis assumed to be the same. Figure 4.10 then displays the total fission rates in each target pin.

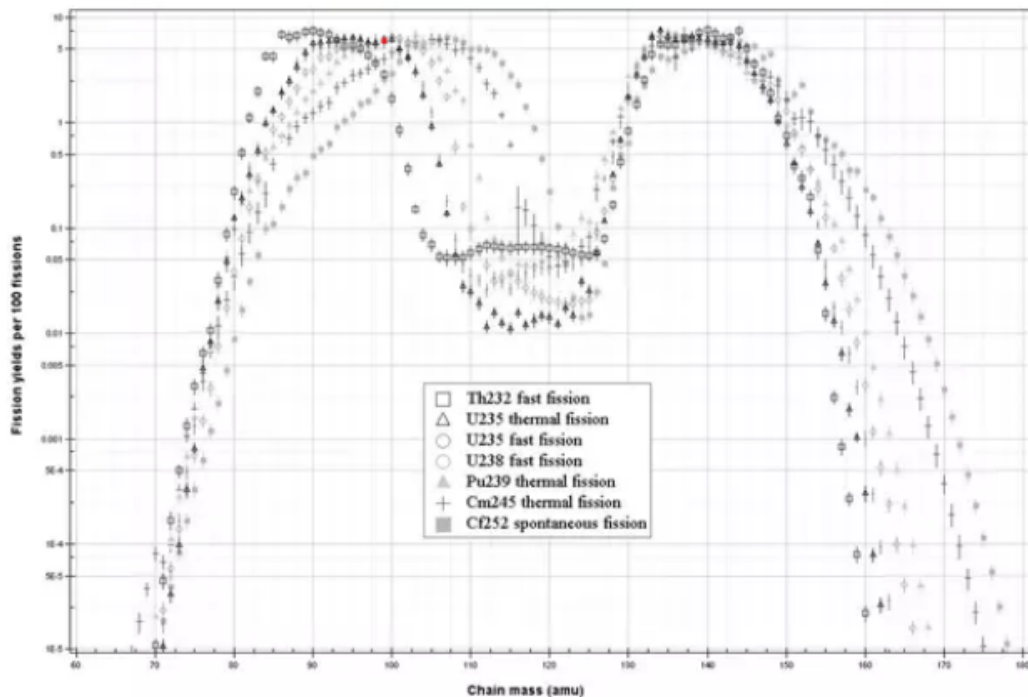


Figure 4.9: Fission product yields for different fission reactions. The red dot marks the ^{99}Mo yield.

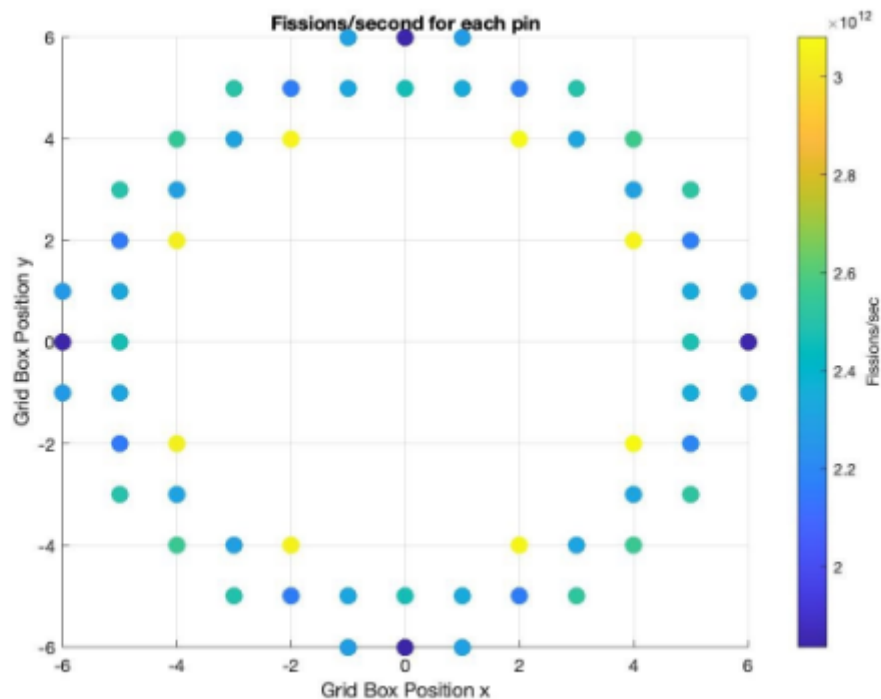


Figure 4.10: Color bar plot of fissions per second in each target pin

By taking the total number of fissions per second in the assembly and inputting into the rate equation, equation (3.2), the total ^{99}Mo production came out to be only 36.7 6-day curries per week. This production rate is far below the project goal of 450 6-day curies per week. Section 4.8 analyzes the failures of this design and suggests ways to improve upon it. It is also important to note that the estimated 6-day curie value is an overestimation of the actual production rate implying that this value may be even more incorrect. Fission product build up would drastically reduce the multiplication factor of the assembly as the irradiation time progresses. Determining the steady state fission rate while fission product build up is driving multiplication down and then in turn reducing fission product concentration is incredibly difficult to effectively model in MCNP. Solving the two coupled equations was beyond our skills and left for future work, possibly through a different activation code.

4.7 Reasons for Failure

Due to the failure of this solid target design, analysis was performed to understand why the ^{99}Mo production rates were so low. One key feature that was immediately apparent was the extent of the targets versus the geometry and distribution of source particles. The tritium gas container extends 100 cm tall while the UO_2 region of the targets is only 49cm, which indicates that a lot of the source neutrons were not being used to induce fission. A fission tally in each uranium target was conducted with a nonu card active in MCNP. This card prevents the production of neutrons during fission so the tally only counts fissions induced by source neutrons. The calculation indicated that only 18.87% of source neutrons were actually utilized by the target assembly to drive subcritical multiplication.

To compare the source neutron utilization with an aqueous subcritical reactor design, a bare 19.75% enriched uranyl nitrate cylindrical reactor was modeled in MCNP. Table 4.8 shows the dimensions and characteristics of the simple aqueous reactor.

Fuel:Water mass ratio	Mixture density [g/cm^3]	Reactor height [cm]	Reactor radius [cm]	k_{eff}
1.22 g $\text{UO}_2(\text{NO}_3)_2$: 1g H_2O	1.101	136	29	0.97283

Table 4.8: Homogeneous UO_2 and H_2O reactor characteristics

The aqueous reactor has a neutron source efficiency of 48.18%, which is over 2.5 times more efficient than the solid target assembly designed in this report. Furthermore,

the source efficiency could be improved further with the addition of reflectors surrounding the reactor fuel.

A solution to improve the utilization of source neutrons in a solid target design would be to expand the coverage of the solid targets. This can be done by either thinning the targets being used or by reducing the uranium density within the targets. Thinning the targets comes at a cost however, as the neutrons born through subcritical multiplication would likely have a larger leakage term. The effects of using a reduced target density would be interesting to investigate as such a design would more closely resemble that of the aqueous water design. It would be difficult to increase the cover of the targets on the core however, as completely covering the accelerator source with solid targets would be a difficult manufacturing challenge. The complex geometry could also increase target loading and unloading times in the assembly.

Design of a subcritical solid target ^{99}Mo production system comes down to two key factors. How efficiently the system utilizes the neutron source, and how well the system takes advantage of subcritical multiplication. To improve on the effectiveness of one aspect of the system, the system would likely have a similar resulting decrease of effectiveness on the other end due to the constraints of using a solid material. Ultimately, the design proposed in this paper's ^{99}Mo production could be improved upon through testing more geometry configurations and Uranium compounds, but it is difficult to imagine such a system competing with an aqueous design. The lower multiplication constant allowed for aqueous subcritical reactors due safety concerns, is ultimately not a problem for the system. The larger homogeneous liquid target is better at efficiently using source neutrons and capturing the neutrons produced in fission. The system also

allows for the removal of fission products during operation which is the nail in the coffin for any solid target subcritical reactor design. While other models using targets are still being constructed, it is very likely that they have key design features that we do not.

Chapter 5

Shielding Analysis

Following the completion of the detailed assembly design, dose rate calculations were conducted to ensure the Mo-99 production facility would be operating within industry standards. Dose rate zoning limits, provided by the IAEA, were the chosen guidelines that were used to determine the required levels of shielding the pool surrounding the neutron accelerator and target assembly. Figure (5.1) shows the IAEA's limitations on access to different levels of radiation.

Access requirement	Design dose equivalent rate ($\mu\text{Sv/h}$)	
	Mean	Maximum
Uncontrolled areas on-site	—	1
Continuous (> 10 person-hours per week)	1	5
1–10 person-hours per week	10	50
< 1 person-hours per week	100	500
1–10 person-hours per year	1000	10 000
< 1 person-hours per year	10 000	^a

^a Dose rates in excess of 10 mSv/h are acceptable provided that the exposure time is correspondingly short.

Figure 5.1: Radiation zoning used to limit time spent in radiation areas [14]

The ultimate goal of the shielding portion of the project is to minimize the equivalent dose rates at the pool top and side of the pool at the same axial location as the center of the assembly. These are the areas likely to achieve the highest dose rates. If these positions can be maintained below the continuous access maximum dose threshold of 0.5 mrem/hr, workers will be free to work without time constrictions anywhere near the irradiation pool.

5.1 Choice of Material

Material selection for shielding is highly dependent on the characteristics of the radiation it is attempting to block. In this case, the shield must both protect against high energy neutrons for the accelerator source, and also the prompt and delayed photons produced through neutron interactions with the uranium targets and the surrounding assembly. Neutrons lose energy through elastic scattering with nuclei, therefore it is necessary to have the proper corresponding materials depending on which energy level of neutrons the system is interacting with. In general, high energy neutrons are shielded by first moderating the neutrons to thermal energies, and then shielding those thermal neutrons appropriately. Equations (5.1) and (5.2) show the average energy loss of a neutron due to elastic scattering with another nucleus.

$$\bar{E} = E_0 \left(\frac{1 + \alpha}{2} \right) \quad (5.1)$$

$$\alpha = \frac{(A - 1)^2}{(A + 1)^2} \quad (5.2)$$

where \bar{E} is the average energy loss of the incident neutron, E_0 is the initial incident neutron energy, and A is the mass number of the nucleus the incident neutron collides with. By inspecting equation (5.2), it becomes apparent that the lower the mass number of the nucleus, the larger average energy loss of the neutron, with of output energies ranging from $E_{min} = \alpha E_0$ to $E_{mas} = E_0$. The lower energy neutrons are then more easily absorbed by materials with high thermal absorption cross sections, while photons on the other hand are most efficiently shielded using high Z materials.

The materials selected to provide shielding ultimately control two aspects of the design: the size/amount of the material necessary to shield effectively, and the overall cost of the system. The size of the shielding pool in this case was ultimately not a large factor in this case as the size of the facility would be more dependent on the size of the extraction, packaging, and shipment space. For that reason, minor reductions in shielding size by the addition of a new material would not be worth an increase in material cost. Water and concrete were selected as the only shielding materials for this facility due to their inexpensive cost and simplicity in design.

5.2 Dose Calculations and Pool Sizing

Once the material choices were established, the next step was to run dose calculations with varying dimensions of the pool. Shielding the top of the reactor pool was done using exclusively light water. This choice was made to allow facility workers to have

access to the targets from above in order to move them from the target assembly to the cooling pit, and ultimately to the extract hot cells from the assembly. The dose at the side of the pool would be reduced by both the water and the concrete container.

An iterative approach was used to determine the necessary depth of the pool to achieve neutron and photon equivalent dose rates below 0.1 mrem/hr. Calculations began with only 50 cm of water covering the top of the neutron accelerator and assembly. As the depth of the water increased, it became increasingly unlikely for neutrons to make it to the pool top and contribute to the flux tally used at the top of the pool to calculate dose. This greatly increased the relative error of the tally, and eventually led to zero score tallies. This problem was initially addressed with a geometry splitting technique was used to divide the pool water into different levels of importance. This technique assigns higher statistical weights to particles that are moving towards the top of the pool. In doing so, the simulation spends more of its computation time on particles that will contribute to the tally score. This method proved to be effective for intermediate depths of water for neutron dose. However, in order to acquire neutron dose at water depths designed to shield photons, a point detector tally was used. This tally is a variance control technique that attributes a tally score to collisions that occur outside of the area of interest. This technique uses a deterministic approach by solving for the scattering angle and energy loss during a collision necessary to acquire a score at the point detector location. By analyzing the probability of the collision contributing to the tally, a modified score can be generated. Figure 5.2 shows the pool top photon dose rates as a function of water depth, as this was ultimately the limiting factor on pool size. It was determined that the depth of the pool needed to be 525 cm (425 cm above assembly) to reduce the equivalent dose to worker to 0.6176 mrem/hr.

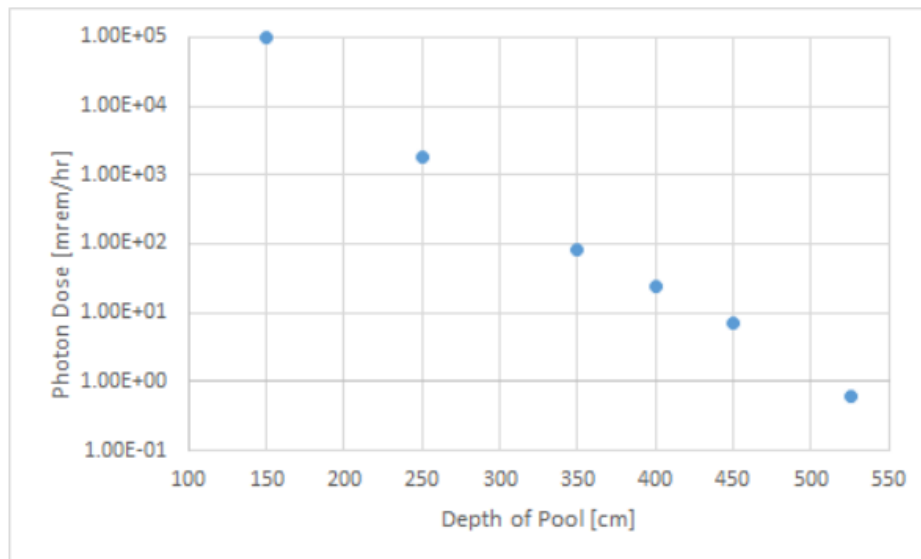


Figure 5.2: Pool top photon dose rates as a function of pool depth

Point detector tallies were also used in a similar fashion to determine the radius of the water and thickness of concrete surrounding the assembly. Due to the increased likelihood of persons working around the base of the pool to perform checks on the neutron accelerator and pool fills, for example, the dose rate on the side of the pool was lowered below 0.1 mrem/hr. By having the radius of the inner wall of concrete be 3m and the thickness of the concrete to be 1m, an equivalent dose to a person of 0.062 mrem/hr was obtained.

5.3 Extraction and Transportation Shielding

Following the irradiation of the samples, the targets are first cooled and then sent to hot cells in order to separate the Mo-99 from the rest of the target. The hot cells are located directly next to the irradiation pool and are transported to the hot cell well below the surface of the water using a transfer system. The system operates similar to a cabinet that can be opened from either side. It is designed to minimize the

amount of water lost in the pool during the transition from pool to hot cell. Any water removed from the pool is sent back in with a pump. The transfer system negates the need for added shielding as the targets move from the reactor pool to the hot cell. Hot cell sizing calculations are not something that can easily be done using MCNP as it is difficult to track fission product build up and activation of the targets. Because of this tracking difficulty, it is impossible to make an accurate source definition to model the irradiated targets. Before determining the wall dimensions, a different activation code, such as Dantsys and ALARA, would be needed to model the radiation energy spectrum and activity being emitted by the activated target.

In the design, the hot cell walls will be composed of high density concrete with fine portions of magnetite aggregate to shield the high energy gamma radiation from fission products [15]. To allow workers to visualize the inside of the hot cell during the extraction process, leaded windows will be installed. The automation of certain processes of the extraction could help reduce dose to workers, though presently there is minimal research surrounding the exact method of doing so. The IAEA has found automation of the Mo-99 to Tc-99m loading process to be economically feasible [16], but more research would need to be conducted to determine whether or not automation could be applied to our extraction technique.

Additionally, shielding the extracted Mo-99 during shipping should be done in a way to conserve space while still keeping workers handling the product safe. Mo-99 decays through β -decay of a mean energy of 389 keV. The most prominent gammas emissions associated with the beta decay are 181 keV and 740 keV photons with 6.05% and 12.2% intensities respectively [17]. Bremsstrahlung X-rays produced as the beta

particles accelerate in the shielding material will also need to be considered in shielding calculations. This means the transport container should be composed of material(s) with a high linear attenuation coefficient at photon energies at and below 740 keV. Figure 5.3 shows the linear attenuation coefficient for common shielding materials as a function of photon energy.

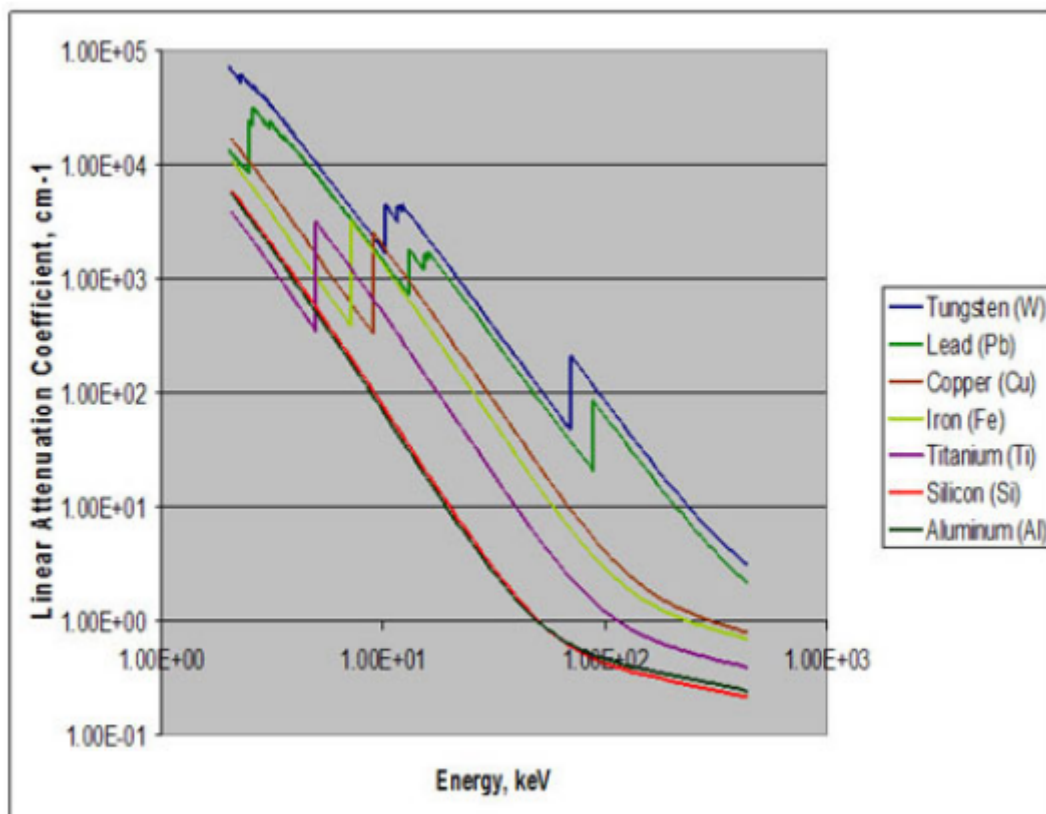


Figure 5.3: Linear attenuation coefficients for shielding materials as a function of energy [18]

From this material analysis, it was determined that Tungsten is ideal the material of choice for our shipping containers as it has a much greater attenuation coefficient at key photon energies of 10 and 100 keV than the other common shielding materials.

5.4 Storage and Transportation of Radioisotopes

The NRC and United States Department of Transportation (DOT) have specific guidelines on the storage and transportation of radioisotopes (spent fuel, nuclear waste and ^{99}Mo) [10]. For nuclear waste and spent fuel, it will be stored in dry casks on-site until it is transported to one of the approved low-level nuclear waste facilities. The spent fuel will be in much lower and activated quantities, but still prevalent as there will be several fission products. Hence, it should be treated as high level waste on-site until it can be transported to the appropriate, NRC-approved facilities. For ^{99}Mo transportation to hospitals, it will follow the NRC guidelines which say to place them in dry casks.

Chapter 6

Thermal Considerations

6.1 Thermal Analysis of the Core

Given the nature of the reactor and the low power needed to operate the core, the thermal analysis of the core was straightforward. Compared to other portions of this project, the workflow was quite simple due to some exploited underlying symmetries in the problem. First, thermal tallies in several different areas were collected through MCNP in order to eventually be used to generate plots. An important note regarding the tallies the uncertainty in the results is proportional to the amount of tallies done. With an increase in tallies, the uncertainty of the results also increases. However, the lower amount of tallies for thermal uses in this case was not necessarily a problem due to the low operating power of the core. After the tallies were recorded in MCNP, post-processing was performed in MATLAB for visualization as displayed in Figure 6.1, with the goal to verify any potential expected symmetries of the system as a whole.

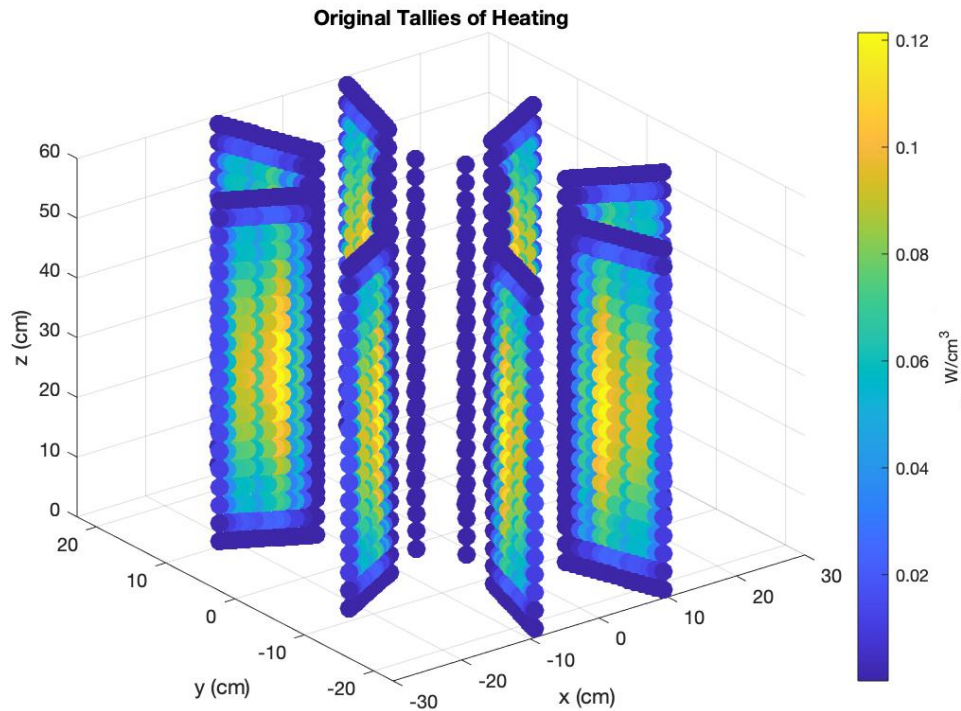


Figure 6.1: Original heat density tallies recorded in MCNP

Based on the image of the initial tallies, the thermal properties can be assumed to be radially symmetric. Because of this symmetry, the analysis can be simplified to a collection of vertical cross-sections, each of which showing the thermal properties at each location. This methodology is very helpful as not only does it effectively lower computational time, but also reduces the amount of uncertainty in the results from the lower amount of tallies done. To conduct further analysis, first, a vertical slice is taken, as seen in Figure 6.2, and then revolved around the entire axis, as seen in Figure 6.3.

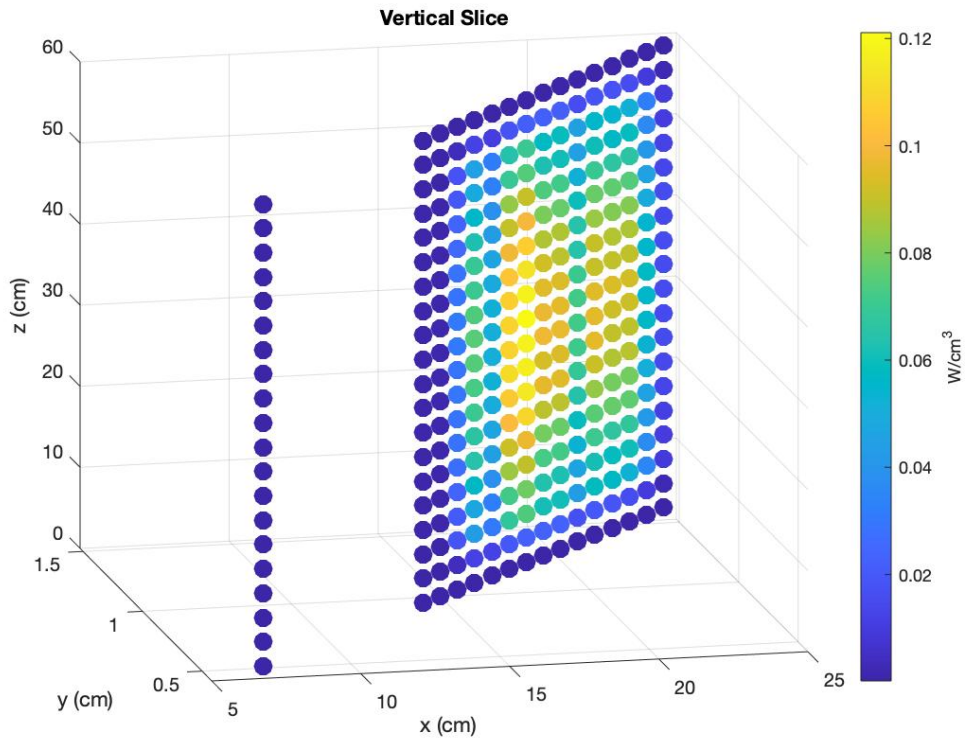


Figure 6.2: A vertical cross-section of the heat density tally

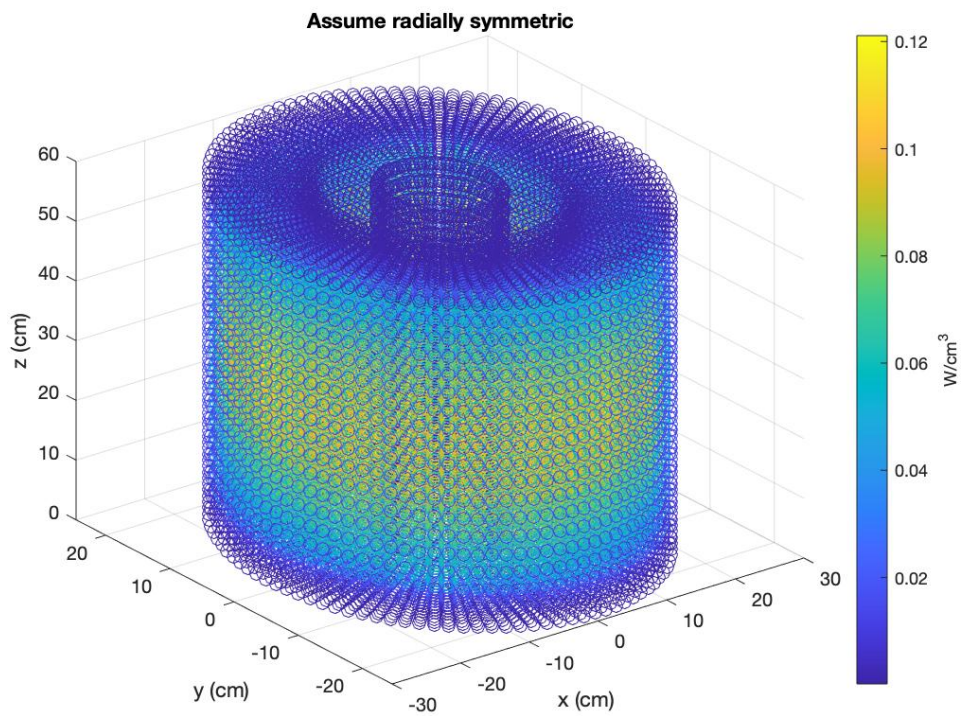


Figure 6.3: The vertical slice of the heat density in Figure (6.2) revolved about the vertical axis

The revolution done in Figure 6.3 is done purely to visualise the image of the core given isotropic heat density. The gap in the space of the tallying is the space where the fuel pins are loaded, and an expected absence in this analysis, as an analysis of the heating of the fuel pins will be conducted shortly. With these symmetries, a robust analysis for different heights on the fuel pins can be conducted, with a specific focus on the vertical symmetry as well. From the vertical cross-section it is also clear that the heat density distribution is also vertically symmetric in addition to being radially symmetric. Therefore, three horizontal cross-sections are taken in Figures 6.4, 6.5, and 6.6 for analysis.

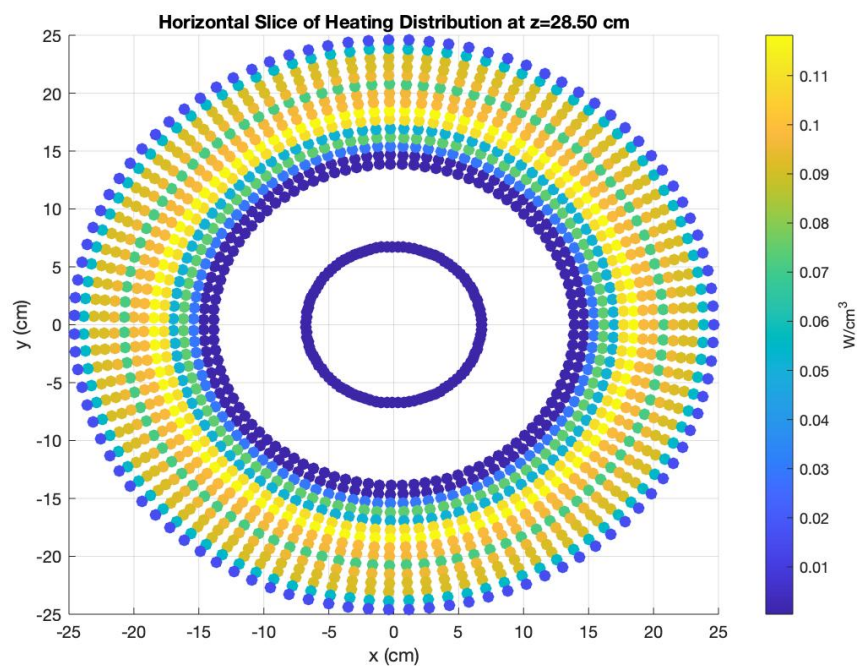


Figure 6.4: The horizontal heat density cross-section at 28.5 cm

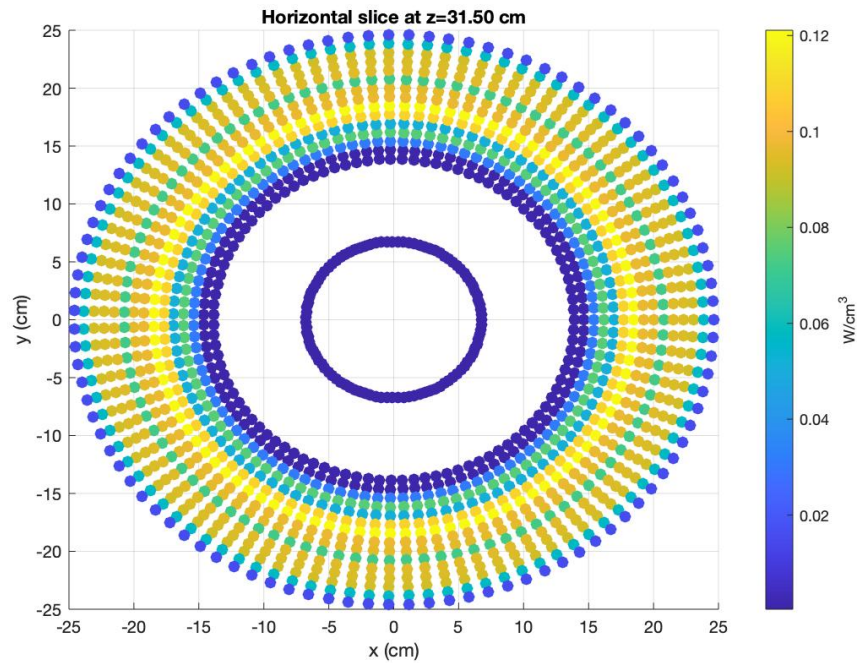


Figure 6.5: The horizontal heat density cross-section at 31.5 cm

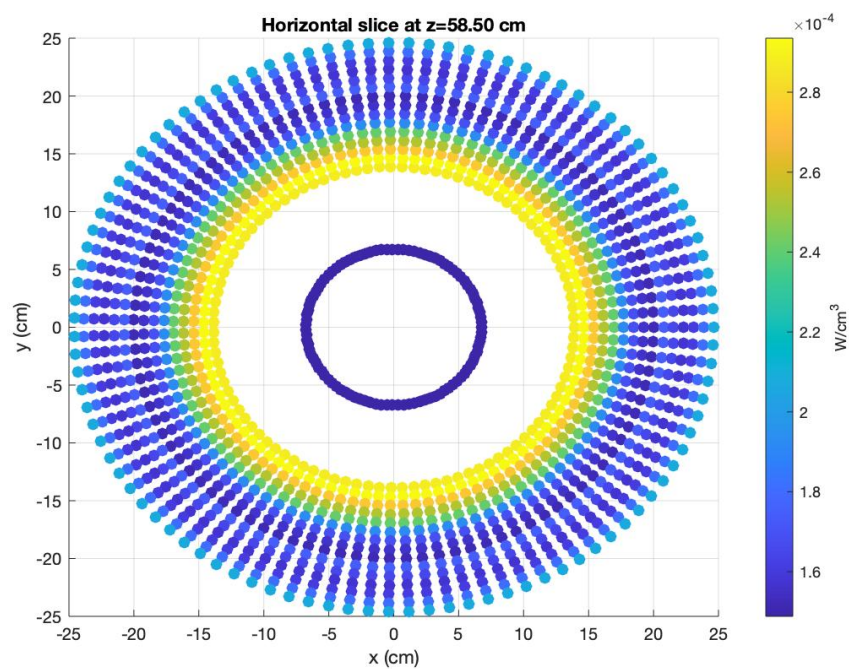


Figure 6.6: The horizontal heat density cross-section at 58.5 cm

Given the very low heat densities displayed in the figures above, the cooling methods used in the design can be simple. From the heating tallies that were conducted across

the entire assembly, the acquired total heat of the system was found to be approximately 4.4 kW. Compared to other ^{99}Mo producing reactors, this quantity is quite low, which is a potential boon for the design.

To acquire the maximum center line temperature for each fuel element, the UO_3 cell in MCNP was segmented in to smaller 1cm long regions. A fission heating tally was run to acquire the power density in W/cm^3 within each section of every cell. The highest power density was only $0.324 \text{ W}/\text{cm}^3$ and found in the 2-4 target. Equation uses 1-D heat transfer to determine the center line temperature for the hottest target assuming uniform $0.324 \text{ W}/\text{cm}^3$ heating. The target only reaches $28.41 \text{ }^\circ\text{C}$.

From this low power, in order to keep the system at an appropriate temperature, a variable heat exchanger is used. The primary heat exchanger has the water from the core exchanging heat with an intermittent loop. The intermittent loop then exchanges heat with water that runs through the city's (in this case Madison) pipes. It should be noted that the design would need to be subtly altered in order to account for varying water main layouts in varying cities. Each loop of the heat exchanger is closed off from one another in order to prevent the risk of radioactive waste to seeping into the city's water system. With each loop being closed off, there have to be two breaks, the primary loop and intermittent loop, in order to ensure maximum public safety. While designing a new heat exchanger is beyond the scope of the project, consulting existing technologies is essential in making the design work properly. After observing a number of different models, we decided that the best suited heat exchanger for the problem would be Grainger's Standard Shell and Tube Heat Exchanger, shown in Figure 6.7 below. One of the most critical features of this option is its heat capacity, which is 1.6 million BTUH, approximately 468 kW, which

is well above our total heat calculated. It is unlikely that the power output of our reactor will ever reach levels where the heat exchanger will fail.



Figure 6.7: Grainger's Heat Exchanger that will be utilized is displayed [19]

The final thermal analysis performed was to analyze the heating of the fuel pins. In Figure 6.8, the fuel pins' heat were calculated and displayed, again using MCNP's tallying features and MATLAB's plotting features. The figure shows the region in which the pins would be located with the concentric circles giving a spatial calibration of the location of the pins. As one would expect, the eight fuel pins closest to the accelerate experience the most heating, with the radial symmetry still being maintained. At the peak, the closest eight pins experience approximately 90 W of power. while the furthest pins located at grid points (6,0), (0,-6), (-6,0) and (0,6) experience approximately 55 W of heating. While these values are relatively small to most nuclear reactors, the heating experienced by the pins is nearly a factor of 10 compared to the heat density dispersed in the surrounding water. Therefore, if a overheating accident were to occur, as unlikely as it would be, the fuel pins would be a likely culprit.

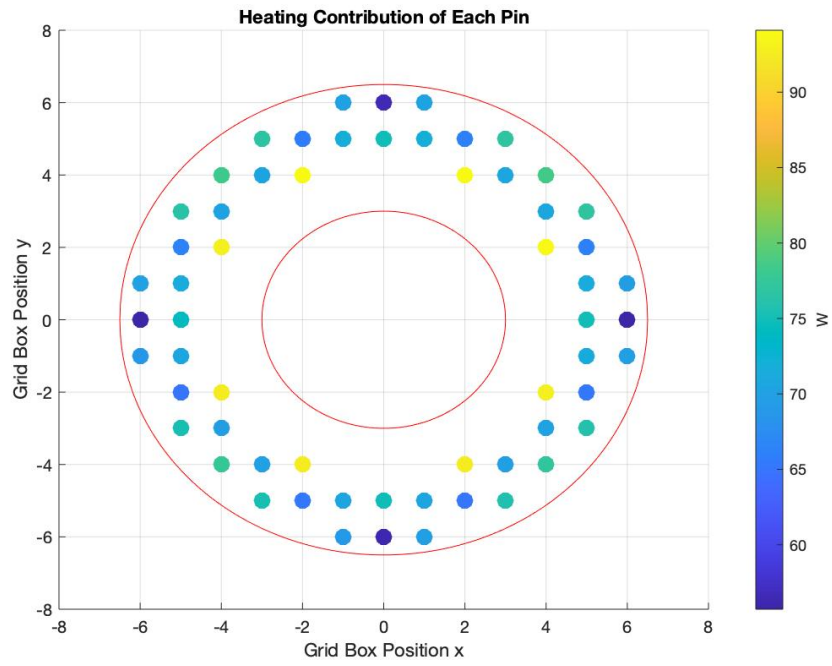


Figure 6.8: The Fuel Pins' in-core heating

Chapter 7

Safety Considerations

Safety is one of the principal considerations in any engineering project, and it is critical to assess different types of safety scenarios, both expected and unexpected. In this section a variety of potential accident situations will be considered and discussed into order to verify the safety of this project.

One of the greatest advantages of the solid target subcritical design has over the subcritical uranium solution reactor is its safety features. The target design uses a UO_2 fuel that has seen decades of extensive use and is deployed in reactors around the world. Extensive research has already been conducted on the use of UO_2 and this design seeks to take advantage of that. The system operates at low fuel temperatures (28.41 °C) and atmospheric pressure (1 atm). This greatly reduces the possibility of fuel cladding failure. Compared to the aqueous reactor design, there is no risk of Uranium precipitating out of solutions and causing a localized criticality accident. Uranium nitrates, the solution used in subcritical reactor design, is also highly acidic with its acidity ranging from 3.4 to 0.2 pH depending on the temperature and mol fraction of the solution [20]. A target-based

system does not have to worry about these hypothetical situations.

The safety analysis proved the solid target subcritical assembly to be a rather robust system capable of handling reactor accident scenarios. In the rare event of target cladding failure, the cooling pit can double as a storage container to prevent the release of fission products. The assembly grid box does not reach even 0.1 dpa until 300 years of continual operation. The 19.75% enrichment of the targets helps reduce ^{239}Pu production over lower enrichment options

7.1 Potential Safety and Accident Scenarios

Due to the low operating temperature and pressure, severe accident scenarios are very improbable. However, in the interest of maintaining absolute certainty of this claim, a number of verification tests have been conducted. The following sections investigate possible accident scenarios and the risks associated with them.

7.1.1 Accidental Loading of Extra Targets

Under normal operation of the irradiation assembly, there are no poisons near the targets during irradiation. Therefore, there is no criticality accident scenario in which a built-in poison corrodes away or a control element is removed from the core. The one reactivity insertion scenario that must be considered is an accidental insertion of an extra uranium target or reflector into the core. It is hard to imagine a reflector element being added to the core as the system does not contain any movable reflector elements, so no arbitrary reflector addition was analyzed. Different potential landing areas for a uranium

target were considered. Figure 7.1 shows the potential landing areas that a criticality calculation was run for. Table 7.1 provides the multiplication factor for each possible accident.

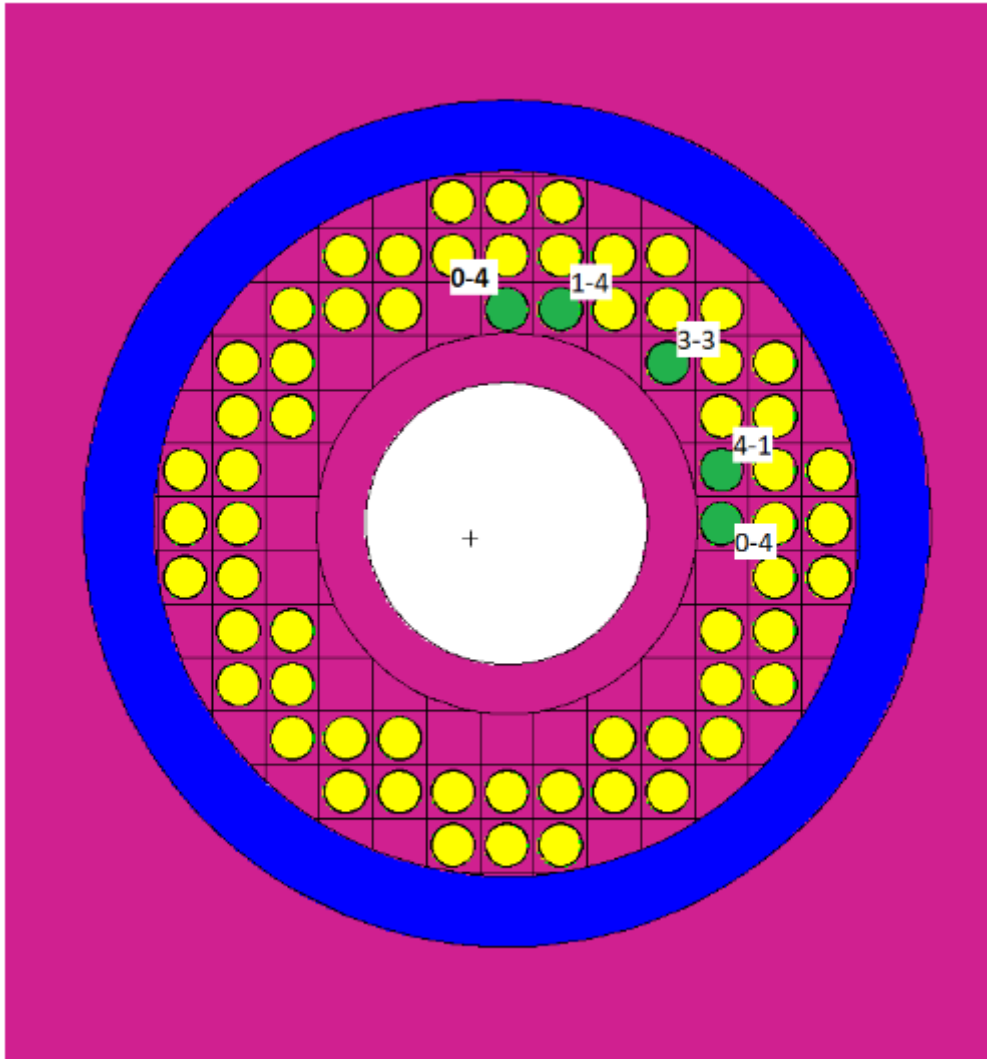


Figure 7.1: The locations of accident scenarios analyzed. Green elements show accidentally inserted targets and the numbers show the corresponding grid location

Target Landing Position [X-Y]	K_{eff}	Standard Deviation	Max K_{eff} at 99% C.I.
0-4	0.99958	0.00077	1.00162
1-4	0.99429	0.00082	0.99645
3-3	0.99087	0.00079	0.99295
4-1	0.99538	0.00080	0.99749
4-0	0.99801	0.00085	1.00026

Table 7.1: Criticality Calculations for accident scenarios described in Figure 7.1

Every location tested for an accidental pin insertion expects the assembly to remain subcritical. The Inhour equation, equation (7.1), was used to predict the reactor period following the worst case scenario of a target landing in the 0-4 position resulting in a multiplication constant of 1.00162.

$$\rho = \frac{l_p}{\tau k_{eff} \cdot \tau} + \sum_{i=1}^6 \frac{\beta_i}{1 + \lambda_i \cdot \tau} \quad (7.1)$$

$$\rho = \frac{k_{eff} - 1}{k_{eff}} \quad (7.2)$$

where

ρ \equiv Reactivity $\left[\frac{\Delta k}{k}\right]$

k_{eff} \equiv Multiplication factor before reactivity insertion [-]

l_p \equiv Prompt neutron lifetime [s]

τ \equiv Resulting reactor period $\left[\frac{1}{s}\right]$

β_i \equiv Delayed neutron fraction of the i^{th} group [-]

λ_i \equiv Decay constant of the i^{th} delayed neutron group $\left[\frac{1}{s}\right]$

Assuming the highest k_{eff} and that the 0-4 pin was inserted into the core instantaneously, the resulting reactor period would be 29.07 s. For a worst case scenario this is not a terribly fast period and should be corrected by an automatic gadolinium nitrate injection (see section 7.2) before the fuel cladding is compromised. The emergency poison injection would reduce the multiplication factor for this accident scenario to 0.934.

7.1.2 Change in Moderator Density

Analysis on the effects of water density on the multiplication factor of the system were conducted to ensure no dramatic reactivity changes as a result of a change in water temperature. Table 7.2 shows the reactivity effects of significant changes to moderator density.

Water Temperature [°C]	Water Density [$\frac{g}{cm^3}$]	k_{eff}	$\Delta\rho$ [$\frac{\Delta k}{k}$]
20	1	0.9867	-
50	0.9847	0.9847	-0.0021
120	0.9823	0.9823	-0.0046

Table 7.2: Reactivity effects of changes to water temperature and density

The system actually displays a slight negative moderator temperature coefficient of reactivity. This is a useful design feature as the system's power increases, the decrease in water density will slightly push the power back down.

7.1.3 Loss of Coolant / Moderator

A loss of coolant accident is not a severe accident for this system. In the event of a complete loss of water, the multiplication constant of the assembly drops to 0.26384. Due to the 4.5 kW power level the system runs at during normal operation, the risk of decay heat causing a meltdown is essentially impossible. An activation code would need to be run to determine the decay heat following shutdown. Then a heat transport code could be used to determine the cladding and UO_2 temperature as a function of time following the loss of water.

The risk associated with a loss of coolant accident for the subcritical assembly is actually the loss in shielding. The water plays a large role in both moderating neutrons to low energies for absorption and attenuation photons. A dose calculation was run to estimate the dose to a person at the pool looking into the core, as well as a person standing directly beside the pool base. Table 7.3 describes the results of this testing.

Position	Photon Dose $\frac{rem}{hr}$	Neutron Dose $\frac{rem}{hr}$	Total Dose $\frac{rem}{hr}$
Pool Top	16.403	1619.4	1635.8
Side of Pool Base	0.5309	2.0525	2.1056

Table 7.3: Dose rates with assembly uncovered

Dose rates for an uncovered assembly while the accelerator is still operating are incredibly high. These numbers are likely underestimates as well as they do not factor shine, the reflection of particles from the ceiling, in the calculation. The NRC's maximum occupational dose for a year, 5 rem, would be exceeded in 11 seconds while working at the top of the pool [21]. An emergency pool fill system will be located in a shielded area of the assembly confinement to allow for emergency cooling and shielding to be initiated without a potential overexposure.

7.1.4 Loss of Heat Sink

The loss of the heat sink is not a particularly risky accident for the system. The specific heat equation, equation (7.3), was used to estimate the time needed to raise the pool temperature 1°C while the accelerator is running.

$$Q = mc\Delta T \tag{7.3}$$

where

Q \equiv Heat energy [W]

m \equiv The mass of water [g]

c \equiv The Specific heat capacity $\left[\frac{J}{g^{\circ}C} \right]$

ΔT \equiv Temperature increase per second $\left[\frac{^{\circ}C}{s} \right]$

The calculation assumed no change in mass of the water and no heat transfer between the water and air or pool container. By determining the temperature increase per second, the time needed operating to increase the pool temperature $1^{\circ}C$ is over 38 hours.

7.2 Safety Poison Injection and Reactor Shutdown Conditions

The irradiation assembly will have 2 safety shutoff features: shutdown of the neutron accelerator, and a gadolinium nitrate poison injection. The automatic shutdown of the accelerator and insertion of gadolinium nitrate will be actuated by the following measurable conditions in table 7.4.

1. A BF_3 fission counter will be placed just outside of the reflector region to measure the neutron population in the reactor. An increase from the normal count rate of the BF_3 detector would likely signify an unintended reactivity insertion into the reactor and possible criticality. When the detector measures a 15% increase over

Condition	Accelerator Shutoff	Gadolinium Nitrate Insertion
Neutron flux exceeding 1.15 times the normal value ¹	Yes	Yes
Loss of high voltage to neutron counter	Yes	No
Inner target temperature exceeds 40°C ²	Yes	Yes
Cooling system outlet temperature exceeds 30°C	Yes	No
Air particulate/gaseous activity above normal level ³	Yes	No
Pool water level changes by more than three inches of normal range (525 cm)	Yes	No
Manual Accelerator Shutoff	Yes	No
Manual Gadolinium Nitrate Insertion	Yes	No

Table 7.4: Conditions initiating either automatic accelerator shutoff of neutron poison injection

the typical flux for fresh (no fission product poisons) target irradiation, the neutron accelerator will shut off and gadolinium poison be injected into the pool to reduce reactivity.

2. One planned method of monitoring fuel temperature would be to instrument one of the sixty target pins used per irradiation batch. A type-K thermocouple would be inserted into the target located in the 2-4 position of the grid box as that is the hottest position in the assembly. If the fuel temperature of the target would rise above 40°C (11.6°C above normal operating temperature), the accelerator would shut down to avoid compromising the cladding of the target element. More analysis would need to be done to see if adding the thermocouple might affect ⁹⁹Mo extraction and assembly neutronics.
3. A continuous gas and particulate air monitor positioned at the top of the pool could provide indication of a fuel cladding breach. Traces of fission product gases including ⁸⁵Kr, ¹³³Xe, and ¹³¹I in the air above the pool would indicate such a breach [22].

Boral carbide control blades and soluble gadolinium nitrate were both considered as emergency reactivity control techniques. Gadolinium nitrate injection was selected to simplify the design of the assembly and allow for easier access to the targets as they will be loaded and unloaded on a weekly basis. Gadolinium nitrate is a commonly used soluble poison in power reactors. It has the highest average cross section of all stable natural elements [23], with high resonances between 1-100 eV. Figure 7.2 shows the gadolinium neutron capture cross section for varying neutron energies.

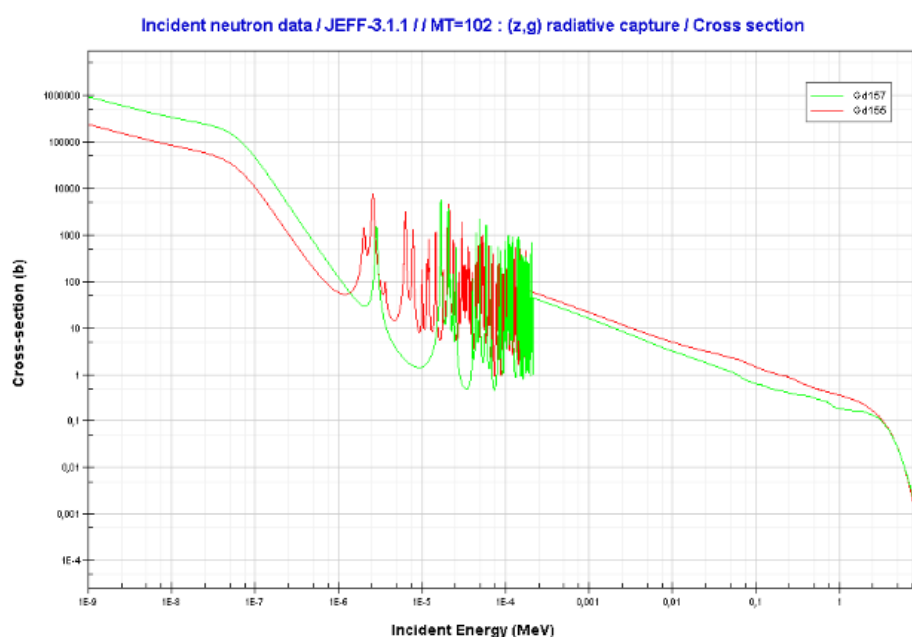


Figure 7.2: Gadolinium neutron cross-section as a function of incident neutron energy

Criticality calculations were conducted to determine a molecular ratio of gadolinium nitrate to water that would be inserted beneath the assembly grid box in order to safely shutdown the reactor in the event of a criticality accident. Ultimately a ratio of 1 gadolinium nitrate molecule per 60,000 water molecules was decided to be sufficient. While this appears to be a low ratio, the large size of the pool requires approximately 47 kg of gadolinium nitrate to be stored for emergency use. Emergency injection into the reactor during normal conditions results in a k_{eff} of 0.926 with a reactivity insertion of

$-0.0804 \frac{\Delta k}{k}$. Such a shutdown would be incredibly costly as the gadolinium nitrate supply would need to be replenished and the gadolinium would need to be filtered from the pool water.

7.3 DPA Analysis

Material corrosion is always a concern when working with high energy neutron fluxes. As high energy neutrons collide with materials in the assembly, they may knock the atoms out of their lattice position. This ultimately compromises the structural stability of the material, limiting the lifetime of the structure. A DPA tally was run to track the number of displacements per atom produced per second of operation, to determine how long the assembly structure could last for. Figure 7.3 shows the results of the mesh tally applied to the target gridbox.

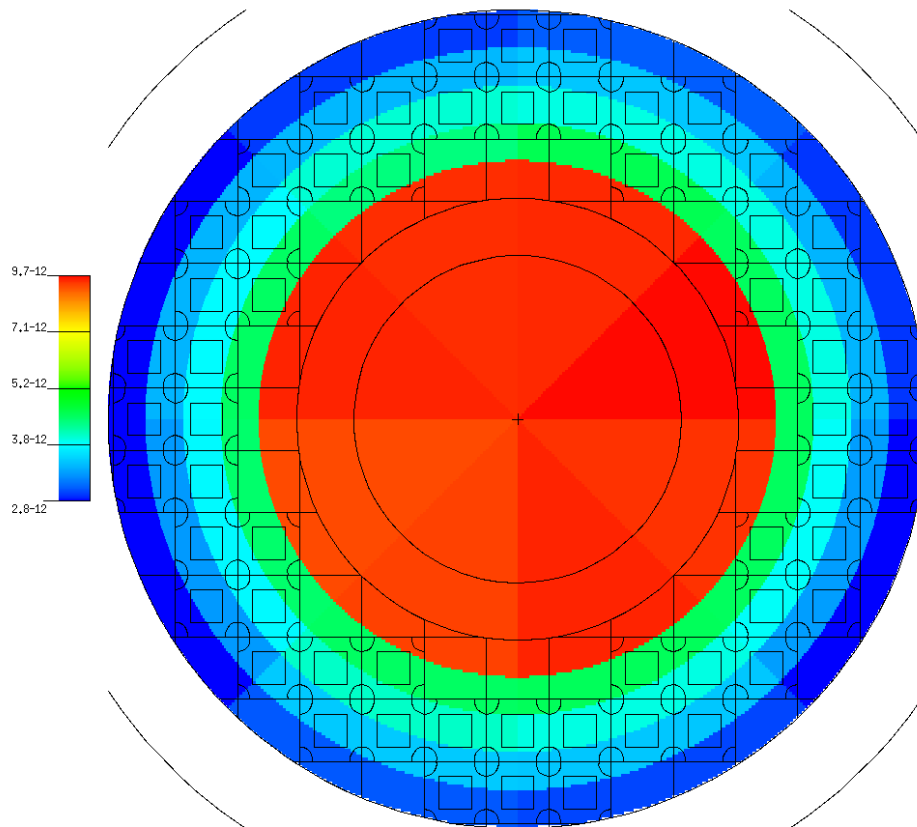


Figure 7.3: The results of the DPA Tally on the Gridbox mesh

The maximum DPA experienced by the target grid box was calculated to be 9.664×10^{-12} DPA/s. A conservative limit of 0.1 DPA was used to determine the lifespan of the target grid box. Even with the conservative limit, the assembly structure could be used for over 300 years before shutting down. The structure will likely outlast the license of the Mo-99 production facility as well as the neutron accelerator.

7.4 Cooling and Storage Pit

The cooling pit is designed to allow for convective cooling of the targets following irradiation. The cooling pit is located at the base of the pool 150cm away from the edge of the outside reflector. The pit separates each target pin with a 1mm layer of boral

carbide sandwiched between two 4.5 mm layers of concrete to maintain the pit sufficiently subcritical. A criticality calculation conducted on the cooling pit shows a multiplication constant of 0.49482 when all 60 target pins are loaded within the cooling pit. Figures 7.4, 7.5, and 7.6 show the geometry of the cooling pit generated via MCNP6's plotting function.

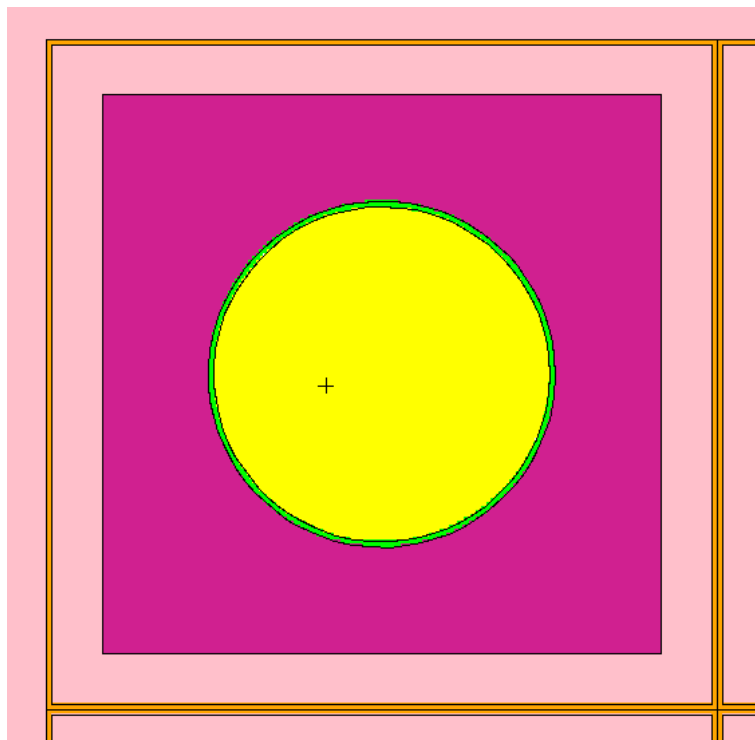


Figure 7.4: Close up of storage pit showing concrete and boron carbide dividers

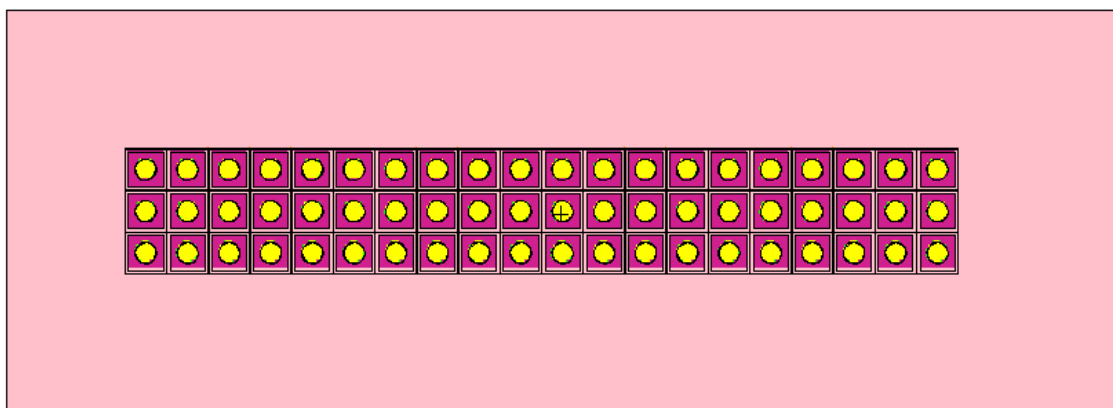


Figure 7.5: Top down view of cooling pit. The pit is 120 cm \times 30 cm

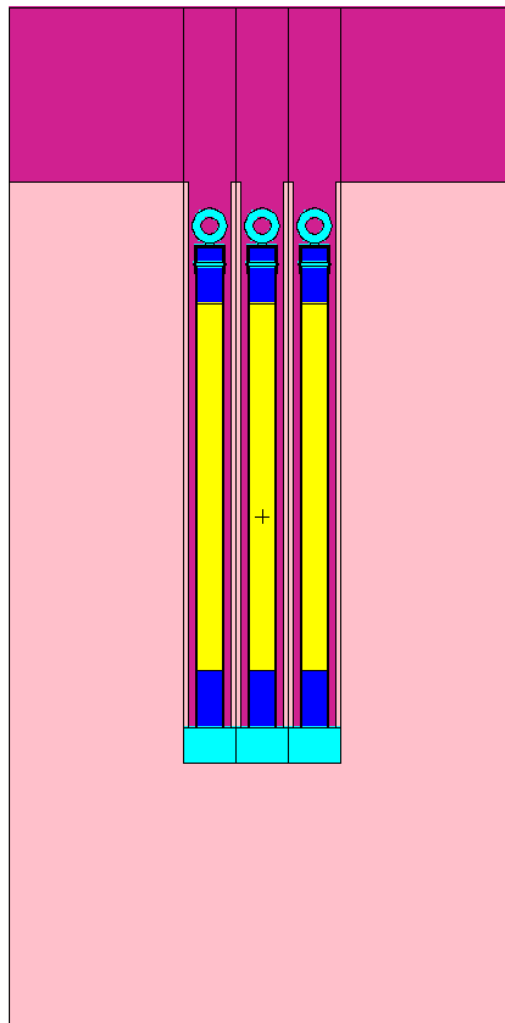


Figure 7.6: Side view of storage pit

The pit depth of 66.55 cm allows the target pin rings to be just barely below the top of the pit. This allows for easier access to the pins following the cooling stage, but also the capability of covering the storage pit with a lead cover. These dimensions can be useful if there is a target cladding breach and the target must be stored to prevent the release of fission products.

7.5 Plutonium Production

A large drawback of the uranium fission based ^{99}Mo production is the radioactive waste byproducts. Of these waste streams, the most difficult and costly isotope to dispose of is ^{239}Pu . ^{239}Pu is a toxic fissile isotope, that in large enough quantities and purity, can be used to produce nuclear weapons. It is produced through neutron capture of ^{238}U . ^{238}U beta decays to ^{239}Np , which then in turn decays to ^{239}Pu with 23.45 minute and 2.36 day half-lives respectively. ^{239}Pu has a half-life of 24,100 years which means significant quantities of ^{239}Pu are lost only through neutron interactions such as neutron capture ($271.5 \text{ b}_{thermal}$) or fission ($747.4 \text{ b}_{thermal}$) [24]. To simplify MCNP calculations, all neutron capture reactions in U-238 were assumed to result in the ^{239}Pu waste. A ^{238}U neutron capture tally was conducted in each target to acquire a ^{239}Pu production rate of 1.89×10^{13} Pu-239 atoms/s of operation. This results in only 4.53 mg of ^{239}Pu produced per batch of ^{99}Mo or 0.239 grams per year.

Research conducted by the IAEA found the use of HEU in ^{99}Mo production reduces ^{239}Pu production by 26 times in conventional reactor production techniques [25]. However, the NRC rules and regulations banned the issuing of licenses to non-power reactors proposing to use HEU [4]. For this reason the design team decided to use the highest possible enrichment for the targets that are still within the LEU limits. One interesting note to add is the potential for Pu to be used in the production of ^{99}Mo . As previously discussed in Chapter 2.2, table 2.1 shows ^{239}Pu has higher fission cross-sections and ^{99}Mo yield percentages compared to conventional ^{235}U fission. However, it is unlikely the NRC would license the civilian use of high quantities of ^{239}Pu so it will not be discussed further in this paper.

Chapter 8

Economic Considerations

8.1 Economic Considerations

The production of ^{99}Mo is primarily done on a large scale, as many of the present production facilities ship their products across the nation, rather than just sell on a local scale. NorthStar Medical Radioisotopes (2018) were the first ^{99}Mo supplier based in the United States in the last three decades. Less than a year later, at least five competitors received aide from the Department to Energy (DOE) to begin taking steps to begin commercial production. Before these events unfolded, the US relied heavily on research reactors that are now beginning to be decommissioned. Of the five companies, four of them received \$15 million grants from the DOE to help complete their projects. The information on construction costs for each company is proprietary, though. One source cites that SHINE Medical Technologies, one of the five competitors, will have construction costs up to \$100 million [26]. The estimates of the cost will hence be assumed to be in the same range as one of the main competitors.

A report by the IAEA gives rough estimates on construction time and costs for LEU facilities. Overall, the time to build a new facility with a processing facility will be around 9-13 years. The selection process takes approximately 2-3 years and the regulatory process takes 1-2 years. The regulatory process consists of drug quality and purity, and commercial sale approval from the FDA, as well as approval by the NRC for the nuclear reactor. Construction would take 6-8 years based on other projects which brings the total time to 9-13 years.

The cost to build a reactor and processing facility will be expensive. One example is the \$20 million to \$50 million ^{99}Mo processing facility that the DOE granted Sandia National Laboratory's nuclear reactor. Once the facility is built, production costs were estimated by a committee by the IAEA. The cost for ^{99}Mo production in 2008 would be about \$225 per 6-day curie with a cost variation of $\pm 40\%$. ^{99m}Tc is produced from technetium generators as a chemical solution. The average cost in 2005 of a 10 Ci generator is around \$1900 with a price variation of 20%. In 2008, the ^{99m}Tc solution was determined to be around $\$11 \pm 20\%$ per dose. Therefore, if the reactor under examination produces 37 6-day curies per batch, and a batch is a week-long irradiation, the total brought in each year from sales of 6-day curies would be approximately \$430,000. The competitiveness of this project compared to other ^{99}Mo producers would be low because of how little 6-day curies it is able to produce while construction costs are high.

Chapter 9

Conclusion

Solid target subcritical ^{99}Mo production was a relevant production technique worth looking into. The design offered improved safety when compared to the aqueous subcritical reactor design and uranium target irradiation in reactor techniques, while not sacrificing specific activity of the final product like other molybdenum production techniques do. Due to the improved safety features over an aqueous subcritical reactor design, the solid target model is capable of operating much closer to criticality in a safe manner. The system builds off of successful research reactor design as simple of a manner as possible. If for no other reason, it was also worth investigating for the lack of research on such a ^{99}Mo production technique. However, some fatal flaws became apparent as the MCNP modeling progressed, and the design proved to be a complete failure. The system is not viable due to the incredibly low production rate of 36.7 6-day curies per week, while using an expensive D-T fusion neutron accelerator device. The solid targets are not expensive enough to take advantage of the full source strength of the accelerator, and are incapable of making up for this with improved subcritical multiplication. The

inability of removing fission products from the system also removes the possibility of irradiating samples for prolonged periods of time without drastic reductions in the neutron multiplication factor. The sections below highlight the features of the system while providing an overview of its strengths and weaknesses.

9.1 Key Design Features

9.1.1 Target Material Choices

The selection of UO_2 fuel for the system may have been made in haste. The higher uranium density of the fuel provides a more tightly packed geometry and promises to reduce fuel waste mass at the end of each batch. This choice comes at the cost of “flexibility” or size of the fuel geometry. Lower density materials would be helpful to utilize more of the source strength in the reactor. While it is not certain that a different form of uranium would improve the production capability of the system, it would have been useful to experiment with different materials at the beginning of the design process. It was proven however, that the maximum LEU enrichment of 19.75% is beneficial for both reducing plutonium product, but also increasing ^{99}Mo production.

9.1.2 Assembly Geometry

The size of the assembly is largely dependent on the fuel type discussed in section 9.1.1. Further lengthening the pins to cover more the accelerator source may begin to cause manufacturing and handling challenges as the targets are already rather thin

(73.0508 cm long versus 1.5 cm radius). Further analysis of the source neutron flux could help move the circle of uranium targets to more optimal radial position away from the source. Testing different radii should be done in future projects to see what balance of conserving neutron flux versus adjusting the neutron energy spectrum the targets experience from the source. It may also be worth while adjusting the lattice positions to provide a more even flux distribution between targets. Our design saw a large discrepancy between the maximum fission rate in the hot pin was 1.68 times higher than that of the coldest pin.

9.1.3 Shielding

The shielding design was selected to be simple, cheap, and corrosion resistant. Water and concrete were sufficient to reduce dose rates below strict IAEA radiation zoning guidelines. The use of geometry in splitting and point detector tallies proved to be incredibly useful variance reduction techniques in determining the dose rates at the pool top and outside the pool base. One large flaw of the cheap shielding technique used was the large radius of the pool water. When running emergency gadolinium nitrate insertion criticality calculations, the required mass of the poison needed to shut down the reactor was calculated to be an enormous, and expensive, 47 kg. A 50 cm reduction of pool radius would decrease the mass of poison stored by 15 kg. The cost reduction of reducing gadolinium nitrate requirements would almost certainly make up for the added cost of incorporating lead into the shielding configuration.

9.1.4 Thermal Analysis

Not much can really be drawn from the thermal analysis section due to the generally low output. The system during normal operation is far removed from any accident situations, but that is more a function of the failure of the design. The system is not producing nearly enough fissions, and for that reason the heating is an incredibly low 4.4 kW.

9.1.5 Safety Analysis

The one aspect where this system really shines is the system's safety. The criticality of the system ($k_{eff}=0.9867$) was adjusted such that even loading an extra pin to the assembly would likely remain subcritical. On top of that accident scenarios such as loss of heat sink and loss of coolant don't appear to be able to cause a fuel cladding rupture. The system incorporates many automatic accelerator shutdown conditions to ensure operation only under normal conditions. The one potential flaw in the safety system would be in the event that the emergency poison needs to be injected. Such an event would be incredibly costly due to the cost of replacing the gadolinium nitrate, but also the time needed to filter the poison from the system. Operational experience would need to occur to see if the convenience of the soluble poison over boron control blade would be worth the potential costs. It ultimately comes down to how many reactivity accidents occur at the facility.

9.1.6 Cost

The cost of constructing the reactor while the limited amount of ^{99}Mo produced is a large drawback. Estimates price the construction costs to be in the range of \$100 million while the design would only bring in approximately \$450 thousand a year. An ideal funding scenario would be that similar to many of the project's competitors: get large funding from the Department of Energy and NRC as these bodies want to promote LEU sources for ^{99}Mo production.

9.2 Future Work and Improvements

Our subcritical solid target ^{99}Mo production design was a complete failure. There is no potential for large scale production of ^{99}Mo , let alone economic incentive, in using such a design. However, if the system were capable of meeting the minimum ^{99}Mo production requirements of the problem statement, this section outlines some of the work that would need to be conducted to further develop our design.

One of the key pieces that is missing in the rate equation and ultimate calculation of ^{99}Mo production is the non-constant multiplication factor of the system. ^{135}Xe and ^{149}Sm fission product poison would cause a significant reduction in the reactivity of the system. An activation code would have to be used to model these fission product concentrations as a function of time, however incorporating this phenomena would likely only further push the solid target system away from viability. From research conducted during the process of designing this system, there is currently no known way to remove these fission product poisons from the fuel during operation. Any reactivity insertion

used to counteract the negative reactivity swing would defeat the purpose of using a subcritical reactor design. Such a feature would mean that the system could potentially go critical and remove the passive safety of the assembly. In that situation it would be more effective to use a critical reactor design as opposed to a solely sub-critical design.

Properly modeling the neutron source could work to the system designs favor. If more accurate accelerator dimensions and fusion distributions are known, the more the assembly geometry could be tailored towards utilizing the source neutrons. Getting in contact with Phoenix and discussing the tritium gas density and source distribution in the chamber could go a long ways towards improving the output and accuracy of the design.

More thermal analysis needs to be done to show that convective cooling would be sufficient means of removing decay heat from targets while in the storage pit. This consideration becomes more important if targets needed to be loaded into the storage pit and closed off using a lead cover. This safety precaution would greatly reduce the heat transfer of pins stored in the pit. While this is likely not a significant issue due to the low temperature of the entire system, it should still be investigated.

Finally, the processing of the targets post irradiation could be fleshed out. The logistics of moving 60 uranium targets from the irradiation assembly to the storage pit and ultimately the hot cell every week is not a simple task. This process may extend the decay time between removal from the reactor and the samples being ready to ship. Activation calculations must also be done to size the dimensions for the hot cell. Then the question remains how can the waste products be used, recycled or disposed of? Other fission product isotopes such as ^{131}I are also used in medical procedures. If the extraction

process could be used to separate out all of the useful isotopes, the potential for the system would be improved. Recycling spent uranium would also reduce the cost of disposal of targets. These considerations are more chemical engineering problems, but are worth asking if the system would ever be deployed.

Chapter 10

Acknowledgements

The NTP team would like to acknowledge the following individuals for their support throughout this project:

- John Murphy - For general advice, oversight, and direction with the project
- Tim Bohm - For continued assistance with MCNP6
- Our parents - For providing us a place to work during the pandemic

Bibliography

- [1] S. N. Laboratories, “Moly 99 reactor could lead to u.s. supply of isotope to track disease”, *Science Daily*, Jun. 2014. [Online]. Available: <https://www.sciencedaily.com/releases/2014/06/140616204040.htm>.
- [2] E. National Academies of Sciences and Medicine, *Opportunities and Approaches for Supplying Molybdenum-99 and Associated Medical Isotopes to Global Markets: Proceedings of a Symposium*. The National Academies Press 500 Fifth Street, NW Washington, DC 20001: The National Academies Press, Feb. 2018, ISBN: 978-0-309-46627-1. [Online]. Available: https://www.ncbi.nlm.nih.gov/books/NBK487245/pdf/Bookshelf_NBK487245.pdf.
- [3] D. Brouillette, *Exports of u.s-origin highly enriched uranium for medical isotope production: Certification of insufficient supplies of non-highly enriched uranium (heu)-based molybdenum-99 for united states domestic demand*, Notice, Jan. 2020. [Online]. Available: <https://www.federalregister.gov/documents/2020/01/21/2020-00902/exports-of-us-origin-highly-enriched-uranium-for-medical-isotope-production-certification-of>.
- [4] U. S. N. R. Commission, §50.64 *Limitations on the use of highly enriched uranium (HEU) in domestic non-power reactors*. U. S. N. R. Commission, Ed. United States Nuclear Regulatory Commission, Feb. 1986. [Online]. Available: <https://www.nrc.gov/reading-rm/doc-collections/cfr/part050/part050-0064.html>.
- [5] ———, §50.2 *Definitions*, U. S. N. R. Commission, Ed. United States Nuclear Regulatory Commission, Aug. 1956. [Online]. Available: <https://www.nrc.gov/reading-rm/doc-collections/cfr/part050/part050-0002.html>.
- [6] N. E. Agency, *The Supply of Medical Radioisotopes: 2018 Medical Isotope Demand and Capacity Projection for the 2018-2023 Period*. ORGANISATION FOR ECONOMIC CO-OPERATION and DEVELOPMENT, 2018. [Online]. Available: <https://www.oecd-nea.org/cen/docs/2018/sen-hlgmr2018-3.pdf>.
- [7] *Deuterium Tritium (DT) Neutron Generator: Alectryon Neutron Generator*, en-US, Library Catalog: phoenixwi.com. [Online]. Available: <https://phoenixwi.com/neutron-generators/high-flux-neutron-generator/dt-high-yield-neutron-generator/> (visited on 05/07/2020).
- [8] *NRC: Fuel Fabrication*. [Online]. Available: <https://www.nrc.gov/materials/fuel-cycle-fac/fuel-fab.html> (visited on 05/08/2020).

- [9] N. R. C. (C. o. M. I. P. W. H. E. Uranium, *Molybdenum-99/Technetium-99m Production and Use*, en. National Academies Press (US), 2009, Publication Title: Medical Isotope Production without Highly Enriched Uranium. [Online]. Available: <https://www.ncbi.nlm.nih.gov/books/NBK215133/> (visited on 05/08/2020).
- [10] *NRC: Backgrounder on Transportation of Spent Fuel and Radioactive Materials*. [Online]. Available: <https://www.nrc.gov/reading-rm/doc-collections/factsheets/transport-spentfuel-radiomats-bg.html> (visited on 05/08/2020).
- [11] I. A. E. Agency, *Non-HEU Production Technologies for Molybdenum-99 and Technetium-99m*. Internat. Atomic Energy Agency, 2013. [Online]. Available: https://www-pub.iaea.org/MTCD/Publications/PDF/Pub1589_web.pdf.
- [12] Y. Lu, G. Zhou, F. A. Hernández, P. Pereslavytsev, J. Leppänen, and M. Ye, “Benchmark of Serpent-2 with MCNP: Application to European DEMO HCPB breeding blanket”, en, *Fusion Engineering and Design*, vol. 155, p. 111583, Jun. 2020, ISSN: 0920-3796. DOI: 10.1016/j.fusengdes.2020.111583. [Online]. Available: <http://www.sciencedirect.com/science/article/pii/S0920379620301319> (visited on 05/08/2020).
- [13] *Nuclear Energy*, en. Elsevier, 2020, ISBN: 978-0-12-812881-7. DOI: 10.1016/C2016-0-04041-X. [Online]. Available: <https://linkinghub.elsevier.com/retrieve/pii/C2016004041X> (visited on 05/08/2020).
- [14] *Radiation Protection Aspects of Design for Nuclear Power Plants*, en, Text, Library Catalog: www.iaea.org Publisher: IAEA, Nov. 2017. [Online]. Available: <https://www.iaea.org/publications/7293/radiation-protection-aspects-of-design-for-nuclear-power-plants> (visited on 05/08/2020).
- [15] A. S. Ouda, “Development of high-performance heavy density concrete using different aggregates for gamma-ray shielding”, en, *Progress in Nuclear Energy*, vol. 79, pp. 48–55, Mar. 2015, ISSN: 0149-1970. DOI: 10.1016/j.pnucene.2014.11.009. [Online]. Available: <http://www.sciencedirect.com/science/article/pii/S0149197014002960> (visited on 05/07/2020).
- [16] I. A. E. Agency, *Radioisotope handling facilities and automation of radioisotope production*. Internat. Atomic Energy Agency, 2004. [Online]. Available: https://www-pub.iaea.org/MTCD/publications/PDF/te_1430_web.pdf.
- [17] *Decay Radiation Results*. [Online]. Available: <https://www.nndc.bnl.gov/nudat2/decaysearchdirect.jsp?nuc=99M0&unc=nds> (visited on 05/07/2020).
- [18] *Attenuation Coefficient*. [Online]. Available: <https://www.nde-ed.org/EducationResources/CommunityCollege/Radiography/Physics/attenuationCoef.htm> (visited on 05/07/2020).
- [19] *Shell and Tube Heat Exchanger, 316 Stainless Steel, Length (In.) 41.125, Width (In.) 7.75*, en, Library Catalog: www.grainger.com. [Online]. Available: <https://www.grainger.com/product/STANDARD-XCHANGE-Shell-and-Tube-Heat-Exchanger-5TNW9> (visited on 05/07/2020).
- [20] J. Botts, R. Raridon, and D. Costanzo, *Density, Acidity, and Conductivity Measurements of Uranyl Nitrate/Nitric Acid Solutions*. Oak Ridge National Laboratory, Oct. 1978. [Online]. Available: <http://citeseerx.ist.psu.edu/viewdoc/download?doi=10.1.1.1006.3107&rep=rep1&type=pdf>.

- [21] *NRC: 10 CFR 20.1201 Occupational dose limits for adults*. [Online]. Available: <https://www.nrc.gov/reading-rm/doc-collections/cfr/part020/part020-1201.html> (visited on 05/07/2020).
- [22] *Measurement of fission product gases in the atmosphere - ScienceDirect*. [Online]. Available: <https://www.sciencedirect.com/science/article/pii/S0168900296007875> (visited on 05/07/2020).
- [23] *Gadolinium*, en-US, Library Catalog: www.nuclear-power.net. [Online]. Available: <https://www.nuclear-power.net/glossary/gadolinium/> (visited on 05/07/2020).
- [24] *Cross Section Table (94-Pu-239)*. [Online]. Available: <https://www.ndc.jaea.go.jp/cgi-bin/Tab80WWW.cgi?/data/JENDL/JENDL-4-prc/intern/Pu239.intern> (visited on 05/07/2020).
- [25] *Management of Radioactive Waste from 99MO Production*, en, Text, Library Catalog: www.iaea.org Publisher: IAEA, Feb. 2019. [Online]. Available: <https://www.iaea.org/publications/5348/management-of-radioactive-waste-from-99mo-production> (visited on 05/08/2020).
- [26] *Nuclear stress test isotope will be made in Wisconsin by Shine Medical*. [Online]. Available: <https://www.jsonline.com/story/money/business/health-care/2019/10/23/nuclear-stress-test-isotope-made-wisconsin-shine-medical/3829367002/> (visited on 05/08/2020).

Appendix A

MATLAB Code

A.1 Plotting Thermal Tallies

```
clear;close all;clc

data=xlsread('Book2.xlsx');

r=data(:,1);
z=data(:,2);
th=data(:,3);
heat=data(:,4);

%%
% [X,Y,Z]=cylinder(r);
r_unique=unique(r);

% figure
% for i=1:length(r_unique)
%     [X{i},Y{i},Z{i}]=cylinder(r_unique(i));
%     surf(X{i},Y{i},Z{i})
%     hold on
% end
```

```
theta=2.*pi.*th;
[x,y,z]=pol2cart(theta,r,z);
figure;
fig1=scatter3(x,y,z,100,heat,'filled')
xlabel('x (cm)')
ylabel('y (cm)')
zlabel('z (cm)')
title('Original Tallies of Heating')
h = colorbar;
set(get(h,'label'),'string','neutrons/cm^3');

th_unique=unique(th);
finder=find(th==th_unique(1));

heat_th=heat(finder);
r_th=r(finder);
th_th=th(finder);
z_th=z(finder);
[x_th,y_th,z_th]=pol2cart(th_th,r_th,z_th);

figure;
fig2=scatter3(x_th,y_th,z_th,100,heat_th,'filled')
xlabel('x (cm)')
ylabel('y (cm)')
zlabel('z (cm)')
title('Vertical Slice')
h = colorbar;
set(get(h,'label'),'string','W/cm^3');

% z_unique=unique(z);
% finder2=find(z_th==z_unique(1));
% z_z=z_th(finder2);
% x_z=x_th(finder2);
% y_z=y_th(finder2);
% heat_z=heat_th(finder2);
```

```
%
% figure;
% scatter3(x_z,y_z,z_z,100,heat_z,'filled')
%
new_theta=linspace(0.001,2*pi,100);
theta_n=zeros(length(r_th));
% z_n=zeros(length(new_theta));
% heat_n=zeros(length(new_theta));
% r_n=zeros(length(new_theta));

%[x_new,y_new,z_new]=pol2cart(new_theta,r,z);
r_prime=r_th';
z_prime=z_th';
heat_prime=heat_th';
th_prime=th_th';

for i=1:length(new_theta)
    if i==1
        theta_n(:,i)=new_theta(i);
        theta_prime=theta_n(:,i)';

    elseif i==2
        theta_n(:,i)=new_theta(i);
        theta_prime=[theta_prime theta_n(:,i)'];
        r2=[r_prime r_prime];
        z2=[z_prime z_prime];
        h2=[heat_prime heat_prime];
    else
        theta_n(:,i)=new_theta(i);
        theta_prime=[theta_prime theta_n(:,i)'];
        r2=[r2 r_prime];
        z2=[z2 z_prime];
        h2=[h2 heat_prime];
    end
end

end
```

```
[x_new,y_new,z_new]=pol2cart(theta_prime,r2,z2);
figure;
fig3=scatter3(x_new,y_new,z_new,50,h2)
xlabel('x (cm)')
ylabel('y (cm)')
zlabel('z (cm)')
title('Assume radially symmetric')
h = colorbar;
set(get(h,'label'),'string','W/cm^3');
saveas(fig3,'Fullrev.png')

z_unique=unique(z_new);
finder2=find(z_new==z_unique(length(z_unique)/2));
z_z=z_new(finder2);
x_z=x_new(finder2);
y_z=y_new(finder2);
heat_z=h2(finder2);

figure;
fig4=scatter3(x_z,y_z,z_z,50,heat_z,'filled')
xlabel('x (cm)')
ylabel('y (cm)')
zlabel('z (cm)')
title('Horizontal Slice of Heating Distribution at z=28.50 cm')
h = colorbar;
set(get(h,'label'),'string','W/cm^3');

finder3=find(z_new==z_unique(length(z_unique)));
z_z1=z_new(finder3);
x_z1=x_new(finder3);
y_z1=y_new(finder3);
heat_z1=h2(finder3);

figure;
fig5=scatter3(x_z1,y_z1,z_z1,50,heat_z1,'filled')
```

```
xlabel('x (cm)')
ylabel('y (cm)')
zlabel('z (cm)')
title('Horizontal slice at z=58.50 cm')
h = colorbar;
set(get(h,'label'),'string','W/cm^3');

finder4=find(z_new==z_unique((length(z_unique)/2)+1));
z_z2=z_new(finder4);
x_z2=x_new(finder4);
y_z2=y_new(finder4);
heat_z2=h2(finder4);

figure;
scatter3(x_z2,y_z2,z_z2,50,heat_z2,'filled')
xlabel('x (cm)')
ylabel('y (cm)')
zlabel('z (cm)')
title('Horizontal slice at z=31.50 cm')
h = colorbar;
set(get(h,'label'),'string','W/cm^3');

finder5=find(z_new==z_unique((length(z_unique)/2)-1));
z_z3=z_new(finder5);
x_z3=x_new(finder5);
y_z3=y_new(finder5);
heat_z3=h2(finder5);
figure;
scatter3(x_z3,y_z3,z_z3,50,heat_z3,'filled')
xlabel('x (cm)')
ylabel('y (cm)')
zlabel('z (cm)')
title('Horizontal slice at z=25.50 cm')
h = colorbar;
set(get(h,'label'),'string','W/cm^3');
```



```

6      10      -7.87  -200 20 -80          U=2 imp:n,p=1 $ grid box
7      1       -1      #6          U=2 imp:n,p=1
C
C LATTICE OF TARGETS
10 0 -107 U=3 lat=1 fill=-7:7 -7:7 0:0
    2 2 2 2 2 2 2 2 2 2 2 2 2 2 2 2 $7
    2 2 2 2 2 2 1 1 1 2 2 2 2 2 2 2 $6
    2 2 2 2 1 1 1 1 1 1 1 2 2 2 2 2 $5
    2 2 2 1 1 1 2 2 2 1 1 1 2 2 2 2 $4
    2 2 1 1 2 2 2 2 2 2 2 1 1 2 2 2 $3
    2 2 1 1 2 2 2 2 2 2 2 1 1 2 2 2 $2
    2 1 1 2 2 2 2 2 2 2 2 2 1 1 2 2 $1
    2 1 1 2 2 2 2 2 2 2 2 2 1 1 2 2 $0 Numbers refer to gridbox postion in core
    2 1 1 2 2 2 2 2 2 2 2 2 2 1 1 2 2 $-1
    2 2 1 1 2 2 2 2 2 2 2 2 1 1 2 2 2 $-2
    2 2 1 1 2 2 2 2 2 2 2 2 1 1 2 2 2 $-3
    2 2 2 1 1 1 2 2 2 1 1 1 2 2 2 2 $-4
    2 2 2 2 1 1 1 1 1 1 1 2 2 2 2 2 $-5
    2 2 2 2 2 2 1 1 1 2 2 2 2 2 2 2 $-6
    2 2 2 2 2 2 2 2 2 2 2 2 2 2 2 2 $-7
    imp:n,p=1
C  -7 6 5 4 3 2 1 0 1 2 3 4 5 6 7
C
11      0          110 -111 -10 1100          fill=3 imp:n,p=1 $ area filled with lattice
C =====
C
C ===== Key Assembly Components =====
C cell# Mat# Dens Surface Combinations Univ Neutron and Photon Importance
C ACCELERATOR SOURCE
17      0          1100 -10 -109          imp:n,p=1 $source container
C
C GRIDBOX COMPONENTS
18      10      -7.87  -1100 20 1200 -1201 1300 -1301          imp:n,p=1 $ inner legs
19      10      -7.87  -1100 20 1200 -1201 1308 -1309          imp:n,p=1
20      10      -7.87  -1100 20 1208 -1209 1308 -1309          imp:n,p=1
21      10      -7.87  -1100 20 1208 -1209 1300 -1301          imp:n,p=1
22      10      -7.87  -1100 20 1202 -1203 1304 -1305          imp:n,p=1 $ outer legs
23      10      -7.87  -1100 20 1206 -1207 1304 -1305          imp:n,p=1
24      10      -7.87  -1100 20 1204 -1205 1302 -1303          imp:n,p=1
25      10      -7.87  -1100 20 1204 -1205 1306 -1307          imp:n,p=1
12      2       -2.2    111 -200 -10 1100          imp:n,p=1 $ outside reflector
C
C WATER SURROUNDING THE SYSTEM
13      1       -1.0    109 -110 -10 1100          imp:n,p=1 $ water between targets and source
14      1       -1.0     10 -301 -300          imp:n,p=1 $ water surrounding targets top
26      1       -1      #18 #19 #20 #21 #22 #23 #24 #25 -1100 20 -300 imp:n,p=1$ water in bottom region
16      1       -1.0    1100 -10 200 -300          imp:n,p=1 $ water surrounding targets outside
C
C CONCRETE POOL CONTAINER
15      9       -2.3    302 -20 -300          imp:n,p=1 $ concrete bottom
27      9       -2.3    300 -303 302 -301          imp:n,p=1 $concrete sides
28      11 -0.001225 -303 -304 301          imp:n,p=1 $air on top of concrete
C VOID
10000   0          304:303:-302          imp:n,p=0 $ void
C =====
C

```



```

m2 6000.80c 1.0
mt2 GRPH.06T
C
C 19.75% ENRICHED UO2
m3 92235.80c 0.1975 92238.80c 0.8025 8016.80c 2
m5 92235.80c 1 $ U235 for tally
m6 92238.80c 1 $ U238 for tally
C
C ZIRCALOY 4
m4 40000.42c -98.55 50000.42c -1.2 26000.42c -0.18 24000.42c -0.07
C
C STAINLESS STEEL 304
m7 25055.80c 2.0239 24050.80c 0.90591 24052.80c 17.46962 24053.80c 1.98091
    24054.80c 0.49309 28058.80c 6.44574 28060.80c 2.48289 28061.80c 0.10793
    28062.80c 0.34413 28064.80c 0.08764 28058.80c 9.468324 26056.80c
    62.07702278 26054.80c 3.954618458 26057.80c 1.43367605
m100 26000.42c 1 $ Fe used for tally
C
C BORAL
c m8 5010 8.058e-3 5011 3.223e-2 6000 1.007e-2 13027 3.831e-2
C
C CONCRETE
m9 1001.80c 0.0077603 8016.80c 0.0440692 11023.80c 0.0010515 & $
    12000.66c 0.0003078 14000.60c 0.0318374 13027.80c 0.002398 &
    19000.66c 0.0006947 20000.66c 0.0029307 16000.60c 5.765e-5 &
    26000.42c 0.0003132
C
C AISI 1335 STEEL
m10 26000.42c -97.35 25055.80c -1.9 6000.80c -0.33 14000.60c -0.35 16000.60c -0.04 15031.66c -0.035
C
C AIR
m11 6000.80c 0.00015 7014.80c 0.784431 8016.80c 0.210748 $ air
    18036.80c 1.560114E-05
    18038.80c 2.94273E-06 18040.80c 0.0046525
C
C POSITIONED WATER (gadolinium nitrate)
C m1000 7014.80c 3 8016.80c 60009 64000 1 1001 120000
C =====
C
C ===== CRITICALITY CONTROL CARDS =====
c kcode 10000 1.0 50 250 $ sampling information
c ksrc 14 0.0 0 $ source position definitions
c 0.0 14 0.0
c 10 10 25.0
c 14 0.0 -25
c 0.0 14 -25
c 10 10 0
c -19.2 0 25
c 0 -19.2 -25
c prdmp j 20 0 1 20 $ result dump control
C
C =====
C
C ===== SOURCE CARDS =====
SDEF X=d1 Y=d2 Z=d3 ERG=14.1 PAR=1 CEL=17 $ no vec and dir input assumes isotropic source, CEL
c $ card uses rejection sampling technique to only

```

```

c                                     $ accept neutrons in cell 17
c
c POSITION DISTRIBUTION
SI1 -10. 10. $ sampling initial neutron x position
SP1 0 1      $ uniform distribution within region
SI2 -10. 10. $ sampling initial neutron y position
SP2 0 1      $ uniform distribution within region
SI3 -50. 50  $ sampling initial neutron z position
SP3 0 1      $ uniform distribution within region
C
C ENERGY DISTRIBUTION (expiemented with during research, not ultimately used)
c SI4 A 2    9.5 12.5 13.75 14.1 16.25 $ piecewise initial energy sampling [MeV]
c SP4 600 30 40 1000 2000 25 $ relative intensity
c
nps 1e5
prtmp j 1e4 1
dbcn 2j 1 500 1 $ source distribution checks
print 10 40 110 128 $ print source, history, material, and universe info
C
C =====
C
C ===== TALLY CARDS =====
c ***NEUTRON FLUX TALLIES***
C
c neutron flux in source container binned by energy
c f14:n 17      $ neutron flux in source container
c e14 0.625e-6 0.1 20 $ bin flux into 3 energies (thermal,epithermal,fast)
c fm14 1.0e13    $ norm (neut/sec) Phoenix webiste lists 1e13 to 5e13 n/sec
c fq14 f e      $ change tally printout cell/surf down, ebins across top
c
c neutron flux mesh tally across assembly
fmesh104:n geom=cyl origin=0.0,0.0,-60.0 axs=0,0,1 vec=1,0,0
      imesh=10.0 13.5 25.0 30.0 35.0 iints=5 3 5 5 5
      jmesh=120.0 jints=12
      kmesh=1.0 kints=1
      emesh= 0.625e-6 1e-6 5ilog 1 5 10 15
fm104 1.0e13 $ norm (neut/sec) Phoenix webiste lists 1e13 to 5e13 n/sec
c
c
c
c ***FISSION TALLIES***
C
c U235 fissions/s
f24:n (1<10[-7:7 -7:7 0]<11)
sd24 1 $ divisor=1 to avoid getting per cm3
fm24 4.3255e10 5 -6 $U238 atomdensity * source strength, material, neutron capture cross section
c
c U238 fissions/s
f34:n (1<10[-7:7 -7:7 0]<11)
sd34 1 $ divisor=1 to avoid getting per cm3
fm34 1.735e11 6 -6 $U238 atomdensity * source strength, material, neutron capture cross section
c
c
c
c ***TOTAL HEATING TALLIES***
c

```

```

c average photon heating W/cm3 across entire assembly
c fmesh44:p geom=cyl origin=0.0,0.0,-50.0 axs=0,0,1 vec=1,0,0
c     imesh=50 iints=1
c     jmesh=120.0 jints=1
c     kmesh=1.0 kints=1
c fm44 -1.602 0 -5 -6 $ p heating in m0 C=rho*1.602e-13*norm
c
c average neutron heating W/cm3 across entire assembly
c fmesh54:n geom=cyl origin=0.0,0.0,-50.0 axs=0,0,1 vec=1,0,0
c     imesh=50 iints=1
c     jmesh=120.0 jints=1
c     kmesh=1.0 kints=1
c fm54 -1.602 0 -1 -4 $ n heating in m0 C=rho*1.602e-13*norm
c
c mesh neutron heating W/cm3
c fmesh64:n geom=cyl origin=0.0,0.0,-30 axs=0,0,1 vec=1,0,0
c     imesh=13.5 25.0 iints=1 15
c     jmesh=60 jints=20
c     kmesh=1.0 kints=8
c fm64 -1.602 0 -1 -4 $ n heating in m0 C=rho*1.602e-13*norm
c
c mesh photon heating W/cm3
c fmesh74:p geom=cyl origin=0.0,0.0,-30 axs=0,0,1 vec=1,0,0
c     imesh=13.5 25.0 iints=1 15
c     jmesh=60 jints=20
c     kmesh=1.0 kints=8
c fm74 -1.602 0 -5 -6 $ p heating in m0 C=rho*1.602e-13*norm
c
c center line fission heating tally (modified for total fission heating in each pin)
c f17:n (7777<10[-7:7 -7:7 0]<11)
c sd17 1 $ vget units of just watts
c fm17 1.602 $ norm*1.602e-13 wattsec/MeV
c
c
c
c ***DPA TALLIES***
c
c mesh over gridbox [dpa/s]
c fmesh204:n geom=cyl origin=0,0,-35.5508 axs=0,0,1 vec=1,0,0
c     imesh=13.5 25 iints=1 5
c     jmesh=4 jints=1
c     kmesh=1.0 kints=8
c fm204 1e-7 100 444 $ 1e13*.8/(2*40e-6*1e24)
c
c dpa in the legs of the gridbox
c f214:n 18 $ leg cell definition was modified in the dpa calc file to make this tally possible
c fm214 1e-7 100 444
c
c
c
c ***SHIELDING TALLIES***
c
c neutron dose top
c f5:n 0 0 485 2.5
c df5 ic=40 iu=1 fac=1.0e16 $ icrp-74 1996 dose equiv, units=mrem/hour, srcstrength (n/sec)*conversion factor
c

```

```
C photon dose top
c f15:p 0 0 485 2.5
c df15 ic=10 iu=1 fac=1.0e16 $ icrp-74 1996 dose equiv, units=mrem/hour, srcstrength (n/sec)*conversion factor
c
C neutron dose side
c f25Z:n 0 410 2.5
c df25 ic=40 iu=1 fac=1.0e16 $ icrp-74 1996 dose equiv, units=mrem/hour, srcstrength (n/sec)*conversion factor
c
C photon dose side
c f35Z:p 0 410 2.5
c df35 ic=10 iu=1 fac=1.0e16 $ icrp-74 1996 dose equiv, units=mrem/hour, srcstrength (n/sec)*conversion factor
c
c
c
c ***PLUTONIUM PRODUCTION TALLY***
c
c fc404 ~pu239 production (atoms/sec)
c f404:n (1<10[-7:7 -7:7 0]<11)
c sd404 1 $ divisor=1 to avoid getting per cm3
c fm404 1.735e11 6 102 $U238 atombdensity * source strength, material, neutron capture cross section
```